TOWARDS FOUNDATION MODELS FOR ZERO-SHOT TIME SERIES ANOMALY DETECTION: LEVERAGING SYNTHETIC DATA AND RELATIVE CONTEXT DISCREPANCY

Tian Lan* **Hao Duong Le*** **Jinbo Li***
Tsinghua University
{lant23, ljb22}@mails.tsinghua.edu.cn
Lehaoduong.Vn@gmail.com

Wenjun He **Meng Wang**
Huawei
{hewenjun8, wangmeng71}@huawei.com

Chenghao Liu† **Chen Zhang†**
Tsinghua University
twinsken@gmail.com
chenzhang01@tsinghua.edu.cn

ABSTRACT

Time series anomaly detection (TSAD) is a critical task, but developing models that generalize to unseen data in a zero-shot manner remains a major challenge. Prevailing foundation models for TSAD predominantly rely on reconstruction-based objectives, which suffer from a fundamental objective mismatch: they struggle to identify subtle anomalies while often misinterpreting complex normal patterns, leading to high rates of false negatives and positives. To overcome these limitations, we introduce `TimeRCD`, a novel foundation model for TSAD built upon a new pre-training paradigm: Relative Context Discrepancy (RCD). Instead of learning to reconstruct inputs, `TimeRCD` is explicitly trained to identify anomalies by detecting significant discrepancies between adjacent time windows. This relational approach, implemented with a standard Transformer architecture, enables the model to capture contextual shifts indicative of anomalies that reconstruction-based methods often miss. To facilitate this paradigm, we develop a large-scale, diverse synthetic corpus with token-level anomaly labels, providing the rich supervisory signal necessary for effective pre-training. Extensive experiments demonstrate that `TimeRCD` significantly outperforms existing general-purpose and anomaly-specific foundation models in zero-shot TSAD across diverse datasets. Our results validate the superiority of the RCD paradigm and establish a new, effective path toward building robust and generalizable foundation models for time series anomaly detection.

1 INTRODUCTION

Time series anomaly detection (TSAD) is a crucial task in domains such as finance (Ahmed et al., 2016), healthcare (Kaji et al., 2019), industrial monitoring (Lan et al., 2025), and cloud operations (Ren et al., 2019). The accurate detection of rare and unexpected events is vital for ensuring system reliability and safety. Despite recent progress driven by deep learning, most existing approaches are trained in a dataset- and

*Equal contribution.
†Corresponding author.

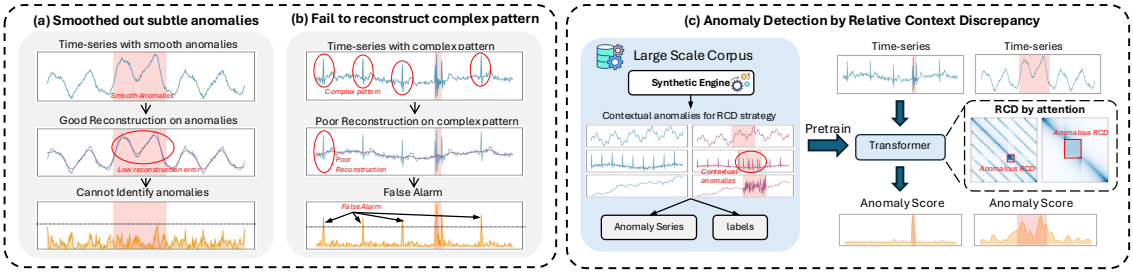

Figure 1: **Limitations of Reconstruction-based TSAD and Our Proposed TimeRCD.** (a) The model accurately reconstructs a smooth anomaly, resulting in a low error score and a missed detection (false negative). (b) The model fails to reconstruct a complex normal pattern unseen in the training dataset, leading to a high error score and a false alarm (false positive). **(c)** TimeRCD adopts RCD with a large-scale corpus and a standard Transformer-Encoder.

model-specific manner, which restricts their scalability and hampers generalization across diverse domains in a *zero-shot* way.

The success of foundation models in natural language processing and computer vision has motivated efforts to establish similar paradigms for TSAD. Existing approaches can be broadly categorized into two directions: (i) general-purpose time series foundation models designed for multiple tasks such as classification, forecasting, and anomaly detection (Gao et al., 2024; Goswami et al., 2024; Woo et al., 2024; Ekambaram et al., 2025; Xie et al., 2024), and (ii) anomaly-specific foundation models tailored explicitly for TSAD (Shentu et al., 2024). The more related work discussion is in Appx. B. Despite their differences, both types of models predominantly rely on reconstruction-based objectives trained on real-world data, where anomalies are inferred indirectly from deviations between reconstructed and observed sequences.

While intuitive, reconstruction models aim to capture dominant patterns rather than detect rare irregularities. This **objective mismatch** introduces fundamental limitations, as shown in Figure 1(a,b). First, subtle and contextual anomalies are often smoothed out, producing low reconstruction error and false negatives. Second, by learning ”average” normal patterns from training data, these models fail to reconstruct complex but normal sequences, leading to false alarms. Such weaknesses are exacerbated in zero-shot settings, where unseen normal patterns make reconstruction-based scores particularly unreliable.

Additional fragilities arise from the limitations of real-world training data. First, labeled anomalies are inherently **scarce**, providing the model with few examples to learn abnormal behavior. Second, training data often lacks **diversity**, covering only a subset of real-world patterns. In zero-shot scenarios, these data limitations leave models unexposed to many unseen normal and abnormal sequences, hindering their ability to generalize and detect novel anomalies. To mitigate these issues, some approaches have focused on data augmentation, where artificial anomalies are injected into real-world time series to enrich the training set (Shentu et al., 2024; Darban et al., 2025; Cai et al., 2024). However, these methods are still fundamentally dependent on the availability and diversity of the underlying real data they seek to enhance. Consequently, in zero-shot and cross-domain scenarios, these data limitations leave models unexposed to many unseen normal and abnormal sequences, hindering their ability to generalize and detect novel anomalies.

To address these limitations, we introduce `TimeRCD`, a novel foundation model for TSAD built on a new pre-training paradigm, as illustrated in Figure 1(c). Our approach abandons indirect reconstruction-based objectives in favor of explicitly learning to detect anomalies through **Relative Context Discrepancy** (RCD). The fundamental insight behind RCD is that many anomalies, particularly subtle or contextual ones, are best identified not in isolation but as a significant discrepancy between the patterns of adjacent time windows. By capturing these relational differences, our model can detect shifts that single-window analysis would otherwise miss.

For our pre-training process, we employ a standard Transformer backbone without any architectural modifications. We treat each time window of a time series as an input token, which allows the self-attention mechanism to naturally compute the inter-token relationships. As shown in Figure 1(c), the model's attention weights learn to capture the discrepancy between contexts, effectively identifying anomalous RCD. An anomaly scoring head then uses these learned discriminative features to produce a final score. To teach the model this explicit detection strategy, we provide it with a rich, supervised signal by first leveraging a synthetic engine. This engine generates a large-scale, diverse, and fully-labeled corpus of time series data that is specifically designed to contain a wide variety of contextual anomalies, enabling the model to learn the RCD task from the ground up. Our main contribution are threefold:

- **The Relative Context Discrepancy (RCD) strategy and the TimeRCD model** We introduce a novel pre-training paradigm for time series anomaly detection that moves beyond reconstruction by explicitly learning to identify anomalies through RCD. This strategy is instantiated in our foundation model, TimeRCD, which uses a standard Transformer to capture relational differences between time windows. This design achieves strong zero-shot generalization through a simple yet powerful architecture.
- **A large-scale, fully-labeled synthetic corpus for foundation models** To enable the RCD pre-training paradigm and its rigorous evaluation, we construct a comprehensive synthetic corpus. It provides token-level annotations for a diverse spectrum of anomalies, including point, contextual, and collective types with cross-variate propagation, offering the essential supervision for building and evaluating zero-shot TSAD models on this corpus.
- **Extensive empirical evaluation** Experiments on diverse corpora demonstrate consistent gains over existing reconstruction-based and general-purpose time-series foundation models. Ablation studies confirm the contributions of both the synthetic corpus and the RCD framework to zero-shot performance.

2 Methodology: The TimeRCD Framework

In this section, we first formally define the zero-shot time series anomaly detection task. We then present the RCD strategy and the foundation model architecture (Section 2.1), which employs an encoder-only Transformer. Finally, we introduce our synthetic data generation engine (Section 2.2), producing a rich, diverse, and precisely annotated training corpus.

Problem Definition For the zero-shot time series anomaly detection problem, we observe a multivariate d-channel time series $\mathbf{X} = (\mathbf{x}_1, \ldots, \mathbf{x}_n)$ with $\mathbf{x}_t \in \mathbb{R}^d$ for each time step $t \in [n] := \{1, 2, \ldots, n\}$. The objective is to produce a binary annotation sequence $\hat{\mathbf{y}} = (\hat{y}_1, \ldots, \hat{y}_n) \in \{0, 1\}^n$ such that $\hat{y}_t = 1$ if and only if time t is anomalous. In the zero-shot setting, the model must detect anomalies on unseen target sequences without any additional training or fine-tuning, distinguishing normal from anomalous behavior.

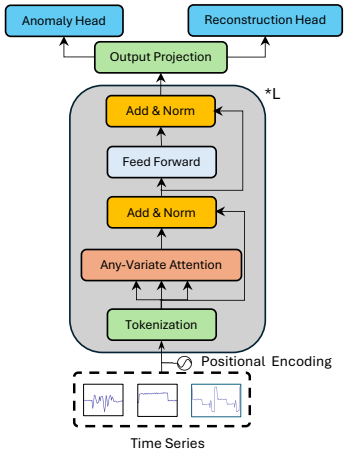

Figure 2: TimeRCD Architecture

2.1 RCD Strategy and Foundation Model Architecture

Relative Context Discrepancy We introduce RCD to redefine zero-shot anomaly detection in time series. Rather than learning discriminative mappings from individual samples to labels, RCD formulates detection as comparing a set of time windows to extract discriminative relational patterns. This approach derives anomaly scores from relational comparisons, enabling the model to detect subtle and comparative anomalies in unseen sequences under the zero-shot setting.

Concretely, when each time window is treated as an input token, the Transformer's self-attention effectively implements RCD: attention weights naturally capture relational discrepancies among windows within the sequence context. This demonstrates that RCD-based anomaly detection can be directly realized using standard Transformer blocks. Building on this, we propose a novel foundation model, TimeRCD, illustrated in Fig. 2, which adopts an encoder-only Transformer (Vaswani et al., 2017) with input tokenization, Transformer blocks, and output projection. Crucially, our approach leverages the existing Transformer architecture directly, requiring no structural modifications, which underscores both its simplicity and broad applicability.

Variate-Window Tokenization We adopt the common practice (Nie et al., 2022) and treat a window of continuous observations as an input token. Since multivariate anomaly detection is a critical task (Zamanzadeh Darban et al., 2024), we build on the design introduced by Moirai (Woo et al., 2024), which flattens multivariate time series so that all variates are represented within a single sequence. This design allows the subsequent Transformer blocks to capture both intra-variate dependencies and inter-variate dependencies. Specifically, given a normalized multivariate time series $\tilde{\mathbf{X}} \in \mathbb{R}^{n \times d}$, we partition it into $\lceil n/W \rceil \times d$ non-overlapping windows, where W denotes the window length. The resulting windows are are then flattened andlinearly projected into input token embeddings $\mathbf{H}_{inp} \in \mathbb{R}^{\lceil n/W \rceil d \times D_v}$.

Transformer Blocks We stack L transformer blocks, each consisting of layer normalization, feed-forward network, and self-attention modules. The architecture imposes no special requirements on the Transformer block itself; however, the self-attention mechanism is repurposed to compute the RCD. Each token attends to other tokens, capturing inter-tokens differences that serve as contrastive features for subsequent anomaly score computation. Specifically, we leverage the any-variate attention (Woo et al., 2024) and formulate the output token embeddings as $\mathbf{H}_{out} \in \mathbb{R}^{\lceil n/W \rceil d \times D_v}$.

Output Projection and Anomaly/Reconstruction Head To derive anomaly scores at the original temporal resolution, the output token embeddings $\mathbf{H}_{out}$ from the Transformer blocks are projected back into the observation space. Concretely, we define two heads during training: $\mathbf{X}_{rec} = \mathbf{H}_{out}\mathbf{W}_s\mathbf{W}_{rec}$ and $\mathbf{X}_{ano} = \mathbf{H}_{out}\mathbf{W}_s\mathbf{W}_{ano}$, where $\mathbf{W}_s \in \mathbf{R}^{D_v \times D_v}$ is the shared embedding projection, $\mathbf{W}_{rec} \in \mathbf{R}^{D_v \times W}$ and $\mathbf{W}_{ano} \in \mathbf{R}^{D_v \times W}$ are the reconstruction and anomaly projection, respectively. The reconstruction head predicts masked portions of the input series, while the anomaly head outputs window-level anomaly scores. Although the reconstruction head is discarded at inference, it acts as a crucial auxiliary task during training, encouraging the transformer blocks to learn rich, stable embeddings beyond pairwise relational discrepancies. This effect is empirically validated in Appx. E.5.1.

2.2 Synthetic Data Generation

We design a synthetic engine to generate multivariate time series with rich, controllable contextual structures, creating a TSAD benchmark that encourages models to recognize anomalies relative to context. The pipeline proceeds in three hierarchical stages: first, defining univariate contextual patterns (Phase 1); next, integrating them into a multivariate system with causal dependencies (Phase 2); and finally, injecting context-aware anomalies that depend on the system's structure (Phase 3). A summary is shown in Fig. 3, with full details in Appx. C.

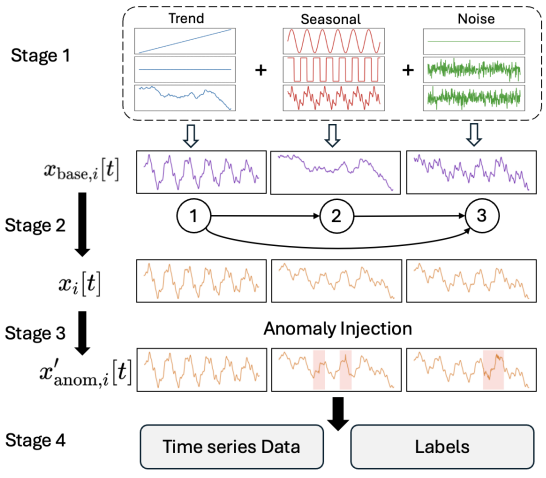

Figure 3: Synthetic data generation procedure.

Stage 1: Context-Template Generation For each channel, we generate normal context data from an additive template: $x_{\text{base}}(t) = T(t) + S(t) + \varepsilon(t), t = 0, 1, \ldots, n-1$. The trend blends deterministic and stochastic components, i.e., $T(t) = (1-\rho_T)\,T_{\text{det}}(t) + \rho_T\,T_{\text{stoc}}(t)$. Seasonality is a mixture of periodic atoms, i.e., $S(t) = \sum_{k=1}^{K} A_k\, w_k(2\pi f_k t + \varphi_k;\, \theta_k)$, where w_k spans sinusoid, square/triangle waves, and wavelet atoms with amplitudes A_k, frequencies f_k, phases φ_k, and shape parameters θ_k. Noise is zero-mean with optional piecewise volatility, e.g., $\varepsilon(t) \sim \mathcal{N}\big(0,\, \sigma^2(t)\big)$ and $\sigma(t)$ allowing bursty segments. The full description for constructing trend and seasonality is in Appx. C.2 and C.3.

Stage 2: Joint-Context Fusion To simulate realistic inter-channel dependencies, we fuse per-channel contexts into a coherent multivariate system via a causal graphical model. We first sample a DAG $G = (V, E)$ over N channels (nodes) and define a latent causal process z_i for each node. Discretizing first-order ODE dynamics by Euler ($\Delta t = 1$) gives an ARX system: $z_i[t] = a_i z_i[t-1] + \sum_{j \in P(i)} b_{ij} x_j[t - \ell_{ij}] + c_i, |a_i| \le 0.8$, with parent set $P(i)$, lags ℓ_{ij}, gains b_{ij}, and bias c_i. The observed signal mixes baseline and causal channels $x_i[t] = (1-\alpha_i)\, x_{\text{base},i}(t) + \alpha_i\, z_i[t], \alpha_i \in [0, 1]$.

Stage 3: Causal-contextual Anomaly Injection Most existing works inject anomalies via simple point-wise corruption or handcrafted signal perturbations—procedures that ignore both temporal context and cross-variate dependencies. We term this class **exogenous injections**, where a multivariate normal system is first generated and then a window in one channel is overwritten, i.e., $x'_{\text{anom},i}[t] = x_i[t] + \Delta(t)$ for $t \in [t_s, t_e)$. Beyond this, we introduce a novel **endogenous injection mechanism** that intervenes prior to causal mixing. Specifically, we perturb the baseline signal $x_{\text{base},i}$ of a parent node, i.e. $x'_{\text{base},i}(t) = x_{\text{base},i}(t) + \Delta(t)$ for $t \in [t_s, t_e)$, allowing abnormal effects to propagate to downstream nodes $x'_{\text{anom},j}[t]$ organically via the ARX dynamics. This process emulates internal system failures and yields multivariate anomalies with coherent temporal and structural footprints. We design more than 20 types of anomalies for $\Delta(t)$ and also consider a type of contextual anomalies which modifies the periodic structure, e.g., replace $S(t)$ with $S'(t)$ to realize frequency or phase shifts within $[t_s, t_e)$. The full taxonomy and parameterizations are detailed in Appx. C.4.

Stage 4: Labels and Masks We generate token-level binary labels per channel. For exogenous injections, positives are exactly the intervention window on the edited channel. For endogenous injections, we label the root-cause window on the source channel and union it with descendant channels after their causal lags, as implied by the DAG and ARX lags $\{\ell_{ij}\}$. This yields two masks: root-cause and propagated effects, supporting evaluation that distinguishes localization from detection. Sequence lengths, DAG sparsity, ARX coefficients, and signal regimes (trend, seasonality, noise) are sampled from configurable priors (Appx. C.1), with all draws fully reproducible. This curriculum generates rich, interpretable dynamics and structured anomalies designed for zero-shot learning.

Relative Context Discrepancy This layered generation process is designed to compel a model to learn RCD. Rather than identifying anomalies via absolute thresholds or isolated patterns, a model must determine whether a data point is abnormal relative to its context. This context is multifaceted, including a variable's own temporal dynamics (e.g., trend, seasonality), its causal relationships with other variables, and the characteristics of the anomaly itself. Our **endogenous anomaly** injection mechanism exemplifies this challenge: a deviation in a downstream "child" variable may be a propagated effect of an upstream "parent" failure. Correctly identifying only the root-cause anomaly requires the model to evaluate multiple variables in light of their causal dependencies. This encourages reasoning beyond simple pattern recognition toward a relational, system-level understanding—the essence of assessing relative discrepancy.

3 EXPERIMENTS

To validate the effectiveness of TimeRCD, we design a comprehensive evaluation to answer three research questions: **RQ1**: How well does TimeRCD perform in strict zero-shot anomaly detection compared with existing time-series foundation models and with full-shot, dataset-specific baselines? **RQ2**: How does the RCD-based strategy exploit long contextual windows, and what is its impact on detecting contextual anomalies and on window-size sensitivity? **RQ3**: How do our synthetic generator and injection design affect performance, and how does accuracy scale with pre-training data size?

3.1 EXPERIMENTAL SETTINGS

Datasets Our evaluation is conducted on a comprehensive suite of 14 public time-series anomaly detection datasets, covering a wide range of real-world and synthetic scenarios. Details about the benchmark datasets can be found in the Appx. D.1.

Baselines We benchmark TimeRCD against methods from two primary settings: (1) **Zero-shot models**, which include our approach and other foundation models (DADA† (Shentu et al., 2024), TS-Pulse (Ekambaram et al., 2025), MOMENT† (Goswami et al., 2024), TimesFM (Das et al., 2024), Chronos (Ansari et al., 2024), Time MOE (Shi et al., 2024)). (2) **Full-shot models**, which are fitted on a per-dataset basis. This category includes deep learning methods (TranAD (Tuli et al., 2022), USAD (Audibert et al., 2020), OmniAnomaly (Su et al., 2019)) and classical statistical algorithms (LOF (Breunig et al., 2000), IForest (Liu et al., 2008)). Note that models marked with (†) were excluded where necessary due to potential data leakage under zero-shot setting. Additionally details about all of the baseslines can be found at the Appx. D.2.

Evaluation Protocol We evaluate model performance using four standard metrics: Affiliation-F1, F1-T, Standard-F1, and VUS-PR. We deliberately avoid using the Point-Adjusted F1 score, as recent work has demonstrated that Point Adjustment (PA) can lead to inflated and misleading performance evaluations (Huet et al., 2022; Wang et al., 2023a). More details about the metrics are shown in the Appx. D.3.

3.2 MAIN RESULTS: TSAD ACCURACY (RQ1)

Our evaluation includes two comparisons: a direct **zero-shot** test against foundation models, and a **full-shot** test against baselines trained on target data. We stress that **TimeRCD** is strictly zero-shot in all settings, testing true out-of-the-box performance. Results are shown in Table 1. In zero-shot comparisons, TimeRCD achieves clear SOTA: on 56 univariate cases it ranks first in **41** and second in **6**. Even against full-shot baselines with access to target data, TimeRCD is highly competitive, ranking first in **28** and second in **5**. This strong showing highlights the power and generalizability of our pre-training framework.

3.3 RCD STRATEGY EFFICIENCY (RQ2)

Qualitative Analysis of Contextual Understanding A key architectural feature of TimeRCD is its ability to process long context windows, allowing it to learn complex temporal dependencies. Many existing zero-shot methods, particularly those based on reconstruction with small look-up windows, are effective at detecting abrupt **point anomalies**—short-term deviations from an immediate pattern (two left charts in Fig. 4). However, these models often fail on subtle **contextual**, where the anomalous behavior is a deviation from a long-term pattern (two right charts in Fig. 4). Their limited context prevents them from distinguishing normal long-term variations from true anomalous segments. In contrast, as our qualitative results in Fig. 4 show, TimeRCD's ability to view the entire series allows it to learn the complex relationships between distant points.

Table 1: Performance of **TimeRCD** against zero-shot and full-shot baselines. TimeRCD operates in a strictly zero-shot capacity in all comparisons. Best result is in **red**, second-best is in blue. Asterisked (*) results are excluded from ranking due to data leaking.

Metric	Model	Univariate Datasets									Multivariate Datasets					Total 1st	Total 2nd
		IOPS	MGAB	NAB	NEK	Power	SED	TODS	UCR	YAHOO	MSL	PSM	SMAP	SMD	SWaT		
Zero-Shot Models																	
Affiliation-F	TimeRCD	83.28	**70.69**	82.48	79.73	**85.51**	**96.87**	86.37	**84.63**	**96.65**	**81.16**	**81.61**	**87.73**	**92.58**	71.55	09	02
	DADA†	89.37*	67.66*	86.56	**95.40**	69.79	65.18	76.89	72.21	92.20*	76.57	81.27	76.92	83.74	**76.18**	02	05
	TS-Pulse	68.76	67.33	70.80	73.05	69.94	67.44	67.90	67.70	70.05	70.14	70.28	69.21	68.21	71.18	00	00
	MOMENT†	87.54*	66.76*	90.45*	92.26	75.97	59.13	59.76	75.77	79.99*	74.55*	65.79	77.42*	74.00*	70.17	00	02
	TimesFM	81.88	66.95	79.73	90.49	69.88	67.14	89.08	70.03	91.28	20.35	71.24	45.44	62.85	44.37	00	01
	Chronos	**90.12**	67.89	**86.66**	93.63	69.72	67.89	**91.96**	74.35	96.34	75.52	70.88	72.22	75.31	70.43	03	04
	Time MOE	76.34	67.23	80.51	80.50	71.19	60.98	54.68	73.56	69.70	69.85	54.74	74.38	69.97	64.37	00	00
F1_T	TimeRCD	28.44	**01.81**	**38.85**	35.87	**28.47**	**69.43**	**65.89**	**34.30**	**85.86**	**42.47**	**37.98**	**33.74**	**53.91**	30.28	11	01
	DADA†	42.50*	00.91*	37.24	47.98	19.80	09.56	35.18	07.22	79.52*	34.58	31.84	30.42	40.80	**35.13**	01	05
	TS-Pulse	04.10	00.81	34.61	27.07	19.90	09.71	13.45	05.12	05.50	23.57	25.39	12.34	09.15	28.58	00	00
	MOMENT†	33.15*	00.80*	52.27*	**63.66**	19.91	09.54	17.47	13.02	11.69*	25.97*	27.77	17.93*	28.68*	28.76	01	02
	TimesFM	**48.95**	00.93	36.74	36.63	19.80	09.58	51.13	10.78	83.46	07.83	25.42	11.64	18.65	21.39	01	01
	Chronos	45.45	01.10	36.10	33.16	19.90	13.18	53.90	10.88	79.00	15.59	25.42	11.72	17.32	28.88	00	03
	Time MOE	25.95	00.63	38.70	15.78	19.85	17.73	20.91	08.29	37.11	23.92	26.82	14.22	19.90	30.11	00	02
Standard-F1	TimeRCD	24.22	**01.62**	**27.70**	33.05	**28.59**	**69.88**	**67.02**	**28.13**	**87.02**	**30.66**	**26.00**	**30.48**	**44.89**	28.73	11	01
	DADA†	32.76*	00.80*	26.91	48.24	15.99	02.69	28.18	03.36	79.30*	22.13	24.07	26.75	34.94	**34.78**	01	05
	TS-Pulse	03.54	00.73	21.61	23.96	18.27	08.84	12.45	02.05	04.00	12.56	22.31	07.44	08.00	23.84	00	01
	MOMENT†	30.69*	00.67*	44.75*	**63.85**	16.39	03.36	14.64	09.00	10.54*	14.43*	23.83	12.92*	29.78*	21.30	01	01
	TimesFM	**34.28**	00.83	26.46	38.15	16.73	02.96	40.08	07.86	84.44	05.75	22.18	10.46	18.65	22.84	01	01
	Chronos	32.69	00.99	26.22	33.54	17.47	08.74	40.52	08.21	78.89	11.63	22.27	09.62	17.50	24.03	00	03
	Time MOE	26.52	00.45	26.20	11.47	12.16	17.73	16.38	04.09	27.50	12.85	24.80	09.01	21.62	23.58	00	02
VUS-PR	TimeRCD	**20.23**	**01.05**	24.32	27.88	**21.25**	**80.75**	**93.46**	**23.09**	84.41	**20.45**	**18.69**	**22.68**	**37.03**	17.58	10	02
	DADA†	24.97*	00.57*	**24.73**	46.85	10.61	06.42	64.83	02.94	70.74*	12.74	17.17	20.02	25.98	**21.13**	02	05
	TS-Pulse	04.64	00.56	16.40	19.39	11.72	09.11	45.86	01.20	09.93	07.41	14.48	03.99	04.56	15.67	00	01
	MOMENT†	37.35*	00.56*	45.38*	**67.74**	10.50	04.31	56.45	06.17	30.81*	09.32*	16.48	08.97*	15.96*	14.90	01	00
	TimesFM	19.56	00.58	24.01	35.02	10.44	06.13	72.89	06.03	**86.78**	11.84	14.76	16.95	13.02	19.43	01	03
	Chronos	19.00	00.60	23.76	31.80	10.95	08.65	70.66	06.56	83.54	08.25	14.61	05.18	10.22	16.44	00	02
	Time MOE	16.63	00.52	22.62	19.76	09.34	10.87	48.78	02.10	20.90	07.82	15.68	04.98	11.12	16.20	00	01
TimeRCD Grand Total (Zero-Shot)																**41**	**06**
Full-Shot Models																	
Affiliation-F	TimeRCD	**83.28**	**70.69**	82.48	79.73	**85.51**	**96.87**	**86.37**	**84.63**	**96.65**	81.16	**81.61**	87.73	**92.58**	71.55	09	01
	TranAD	83.19	67.28	90.28	85.02	71.56	61.03	52.76	73.31	76.08	79.91	73.83	87.39	92.20	**75.37**	01	04
	USAD	71.08	67.81	91.54	71.13	76.48	55.60	47.90	76.00	53.05	81.86	57.86	87.25	85.09	75.06	00	03
	OmniAnomaly	80.32	67.35	**92.35**	**86.30**	78.16	61.26	50.73	73.53	71.31	83.15	58.17	**91.38**	85.82	73.39	03	02
	LOF	81.06	68.44	75.75	84.74	66.76	63.85	60.58	73.53	75.63	**84.35**	61.98	63.32	64.13	56.34	01	02
	IForest	52.81	68.82	39.84	71.15	00.00	70.09	44.17	50.56	33.30	63.36	63.78	59.96	69.71	00.00	00	02
F1_T	TimeRCD	28.44	01.81	38.85	35.87	**28.47**	**69.43**	**65.89**	**34.30**	**85.86**	42.47	**37.98**	33.74	**53.91**	30.28	07	02
	TranAD	22.63	01.65	37.28	69.97	22.36	09.57	13.51	07.75	08.41	39.42	25.49	29.12	37.98	49.58	00	01
	USAD	20.99	**04.07**	**61.46**	70.64	28.23	09.54	20.85	14.63	09.35	48.71	28.96	43.94	50.41	**50.41**	03	05
	OmniAnomaly	**51.17**	01.61	40.09	**82.20**	23.48	09.68	14.33	08.47	24.16	**49.36**	30.42	**46.63**	51.84	46.64	04	04
	LOF	27.97	01.15	35.76	63.57	19.80	09.60	31.63	08.31	55.93	38.97	25.58	21.81	10.13	30.62	00	02
	IForest	07.64	00.84	21.44	65.56	00.00	09.54	11.06	06.36	04.90	20.73	25.39	14.32	16.20	00.00	00	00
Standard-F1	TimeRCD	24.22	01.62	27.70	33.05	**28.59**	**69.88**	**67.02**	**28.13**	**87.02**	30.66	26.00	30.48	44.89	28.73	05	01
	TranAD	**34.85**	01.46	27.33	60.36	22.36	02.63	11.94	04.40	05.70	29.60	25.63	25.11	43.99	61.86	01	01
	USAD	30.66	**03.89**	**56.15**	62.91	28.24	03.41	23.87	10.74	07.21	38.71	28.41	38.66	53.06	**62.82**	03	07
	OmniAnomaly	47.05	01.44	28.81	**74.03**	23.50	00.43	12.65	05.11	21.40	**39.10**	**30.43**	**40.50**	**57.06**	55.93	05	01
	LOF	30.28	01.05	24.04	56.92	12.18	04.11	25.77	04.70	48.95	30.65	18.80	18.70	08.41	29.08	00	03
	IForest	08.37	00.73	29.41	58.10	19.77	03.81	13.35	04.09	03.20	14.68	24.15	13.61	16.89	26.76	00	01
VUS-PR	TimeRCD	20.23	**01.05**	24.32	27.88	**21.25**	**80.75**	**93.46**	**23.09**	**84.41**	20.45	**18.69**	22.68	37.03	17.58	07	01
	TranAD	**21.61**	00.64	24.82	61.63	13.04	05.75	47.33	02.25	25.78	14.78	16.49	13.37	28.34	**47.37**	02	00
	USAD	16.58	00.75	**55.03**	58.53	18.68	04.37	56.36	08.85	14.15	29.95	17.59	26.37	34.53	44.73	01	08
	OmniAnomaly	25.35	00.64	27.17	**74.51**	14.32	06.20	45.55	02.40	29.26	**31.57**	18.58	**28.07**	**37.44**	42.97	04	03
	LOF	19.43	00.57	21.18	58.52	09.31	06.81	49.14	02.39	41.37	24.67	13.58	10.59	04.40	14.50	00	01
	IForest	08.59	00.62	23.57	56.50	11.56	07.71	46.62	02.88	10.47	11.29	15.85	07.55	08.88	15.49	00	01
TimeRCDGrand Total (Full-Shot)																**28**	**05**

Quantitative Analysis of Contextual Understanding We create specialized, unseen datasets containing either purely point or contextual anomalies, ensuring a fair zero-shot evaluation (details in Appx. E.2). The results are in Fig. 5. While TimeRCD's performance on point anomalies is highly competitive with other top zero-shot models, it is substantially superior on contextual anomalies. On this task, our model achieves a `Standard-F1` of 0.827, whereas all other models suffer a significant performance collapse. This performance disparity provides strong evidence that TimeRCD's ability to leverage long-range context is a key capability, allowing it to detect complex deviations that are challenging for methods with a more limited contextual view.

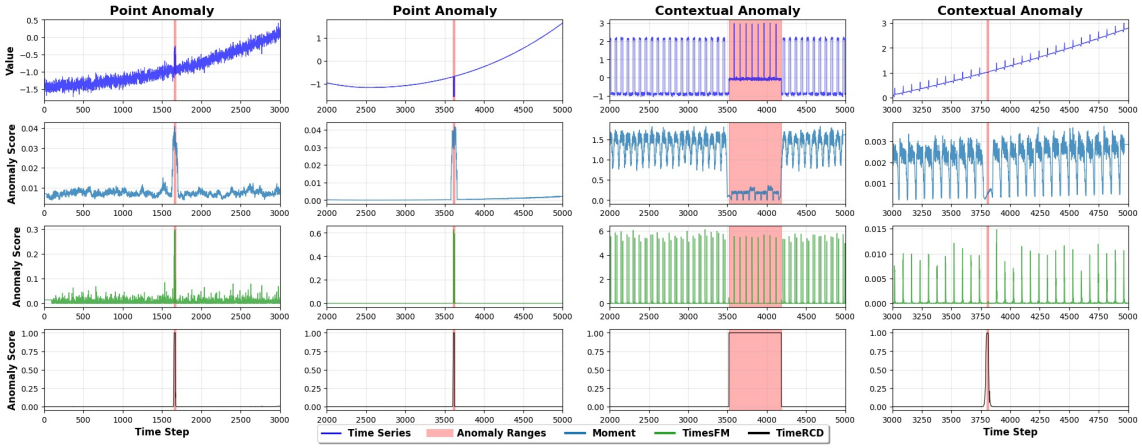

Figure 4: Qualitative comparison of anomaly scores.

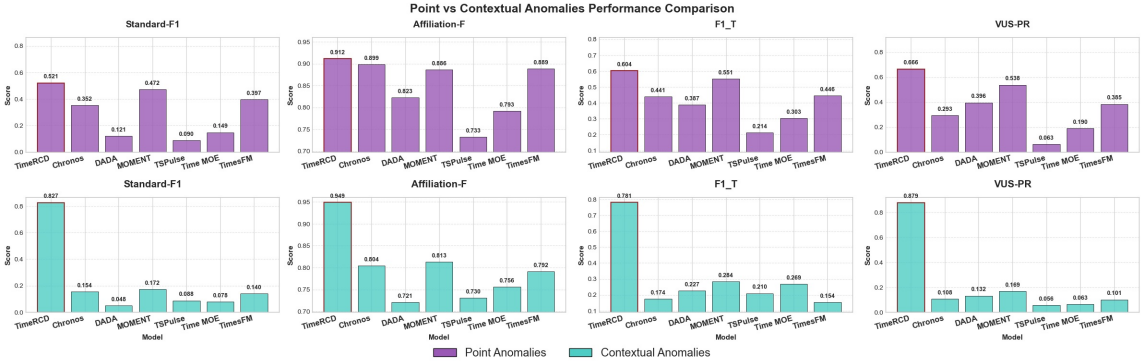

Figure 5: Comparison on specially-created datasets containing either point or contextual anomalies.

Impact of Context Window Size TimeRCD's ability to process variable context lengths is a core architectural feature. To analyze its impact, we evaluate performance with input window sizes from 1k to 13k. As shown in Fig. 6, the results confirm that the optimal context length is task-dependent. For datasets with long-term patterns like **UCR**, **Power**, **SMAP**, and **SMD** Fig. 6 (a, b, d, e), performance generally improves with a larger window, as this allows the model to establish a more robust baseline of "normal" behavior. Conversely, on inherently short series like **YAHOO** Fig. 6(c), performance remains flat, as the series length itself becomes the effective context limit. A detailed breakdown for all datasets is available in Appx. E.3.

3.4 Synthetic Data Efficiency (RQ3)

Ablation Study on Pre-training Data To validate our data generation framework, we train on the same TimeRCD (architecture, hyperparameters, epochs) on three 350M-point datasets, each with 350M points to match the real-world data scale: (1) our synthetic data with *in-context* anomaly injection, (2) the same synthetic series but with DADA-injected anomalies (Shentu et al., 2024), and (3) real-world data (Godahewa et al.) augmented with DADA. Table 2 shows weighted averages over 9 univariate benchmarks (full results in Appx. E.4). Models trained on augmented real data performed far worse, confirming the necessity of a high-quality synthetic curriculum. Comparing the two synthetic variants reveals a key trade-off: though

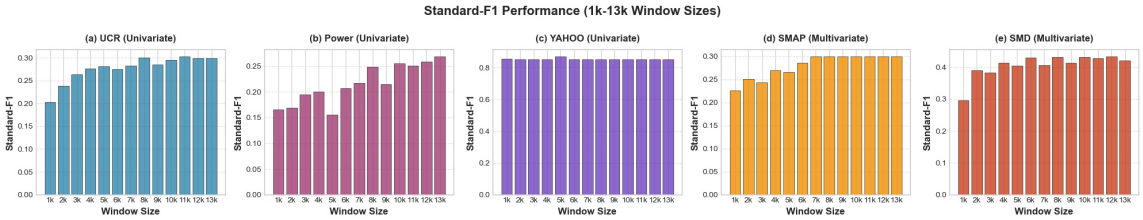

Figure 6: Performance on univariate (top) and multivariate (bottom) datasets as a function of the input window size, varied from 1k to 13k.

using DADA-injection achieves similar Affiliation-F and slightly higher VUS-PR, it causes sharp drops in finer-grained metrics (F1-T ↓6.4%, Standard-F1 ↓6.1%). This indicates our in-context injection generates more challenging and robust training signals.

Table 2: Weighted average performance across 9 univariate benchmarks.

Pre-Training Dataset	Affiliation-F	F1-T	Standard-F1	VUS-PR
Our Synthetic Data	**0.878**	**0.569**	**0.523**	0.478
Our Synthetic + DADA Injection	**0.878**	0.505	0.462	**0.487**
Real-world Data + DADA Injection	0.716	0.073	0.062	0.102

Dataset Scaling To investigate the effect of pre-training data scale on performance, we train TimeRCD on increasingly larger subsets of our synthetic dataset: 350M, 700M, and the full 2.5B data points. The results, shown as a weighted average across our benchmark datasets in the Fig. 7, demonstrate a clear and positive scaling law. As the amount of pre-training data increases, the model's performance consistently improves across all four evaluation metrics.

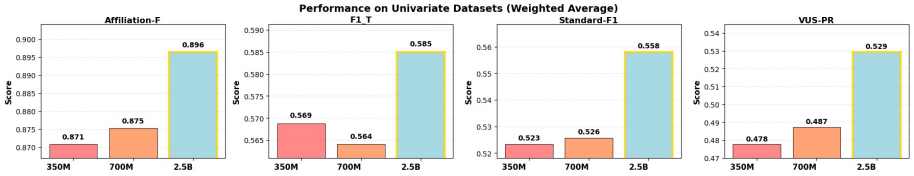

Figure 7: Demonstration of positive scaling laws. The figure shows weighted average performance across our benchmarks when training on datasets of increasing size (350M, 700M, 2.5B).

4 Conclusion

In conclusion, TimeRCD successfully addresses the objective mismatch in reconstruction-based methods by introducing the principle of Relative Context Discrepancy. This work establishes a new and effective pre-training paradigm for zero-shot TSAD, with its conceptual simplicity and strong empirical results opening several promising avenues for future research. Looking forward, the extensibility of our framework invites investigation into efficiently fine-tuning the pre-trained TimeRCD on domain-specific datasets for critical applications. As a current limitation and future direction, our implementation relies on a standard transformer backbone; exploring novel network structures specifically engineered to more efficiently capture RCD could yield further performance gains and is a promising area for subsequent research.

ETHICS STATEMENT

In alignment with the ICLR Code of Ethics, this research is committed to upholding the highest standards of academic integrity, social responsibility, and fairness by proactively identifying and mitigating potential ethical risks, ensuring transparency in methodology and limitations, respecting privacy and consent in data usage, promoting inclusivity and non-discrimination, and avoiding any form of harm or misuse, while fostering a constructive and respectful scholarly environment for all participants and the broader community.

REPRODUCIBILITY STATEMENT

We have made every effort to ensure that the results presented in this paper are reproducible. We ensure reproducibility by fully specifying our synthetic data generator (Appx. C). All evaluation datasets and splits follow the TSB-AD protocol described in Appx. D.1. Training configurations—model architecture, optimization, masking strategy, early stopping, and windowing—are detailed in Appx. D.4.

REFERENCES

Mohiuddin Ahmed, Abdun Naser Mahmood, and Md Rafiqul Islam. A survey of anomaly detection techniques in financial domain. *Future Generation Computer Systems*, 55:278–288, 2016.

Abdul Fatir Ansari, Lorenzo Stella, Caner Turkmen, Xiyuan Zhang, Pedro Mercado, Huibin Shen, Oleksandr Shchur, Syama Sundar Rangapuram, Sebastian Pineda Arango, Shubham Kapoor, et al. Chronos: Learning the language of time series. *arXiv preprint arXiv:2403.07815*, 2024.

Julien Audibert, Pietro Michiardi, Frédéric Guyard, Sébastien Marti, and Maria A Zuluaga. Usad: Unsupervised anomaly detection on multivariate time series. In *Proceedings of the 26th ACM SIGKDD international conference on knowledge discovery & data mining*, pp. 3395–3404, 2020.

Sathya Kamesh Bhethanabhotla, Omar Swelam, Julien Siems, David Salinas, and Frank Hutter. Mamba4cast: Efficient zero-shot time series forecasting with state space models. *arXiv preprint arXiv:2410.09385*, 2024.

Markus M Breunig, Hans-Peter Kriegel, Raymond T Ng, and Jörg Sander. Lof: identifying density-based local outliers. In *Proceedings of the 2000 ACM SIGMOD international conference on Management of data*, pp. 93–104, 2000.

Yifu Cai, Arjun Choudhry, Mononito Goswami, and Artur Dubrawski. Timeseriesexam: A time series understanding exam. *arXiv preprint arXiv:2410.14752*, 2024.

Zahra Zamanzadeh Darban, Yiyuan Yang, Geoffrey I Webb, Charu C Aggarwal, Qingsong Wen, Shirui Pan, and Mahsa Salehi. Dacad: Domain adaptation contrastive learning for anomaly detection in multivariate time series. *IEEE Transactions on Knowledge and Data Engineering*, 2025.

Abhimanyu Das, Weihao Kong, Rajat Sen, and Yichen Zhou. A decoder-only foundation model for time-series forecasting. In *Forty-first International Conference on Machine Learning*, 2024.

Samuel Dooley, Gurnoor Singh Khurana, Chirag Mohapatra, Siddartha V Naidu, and Colin White. Forecastpfn: Synthetically-trained zero-shot forecasting. *Advances in Neural Information Processing Systems*, 36:2403–2426, 2023.

Vijay Ekambaram, Subodh Kumar, Arindam Jati, Sumanta Mukherjee, Tomoya Sakai, Pankaj Dayama, Wesley M Gifford, and Jayant Kalagnanam. Tspulse: Dual space tiny pre-trained models for rapid time-series analysis. *arXiv preprint arXiv:2505.13033*, 2025.

Shanghua Gao, Teddy Koker, Owen Queen, Tom Hartvigsen, Theodoros Tsiligkaridis, and Marinka Zitnik. Units: A unified multi-task time series model. *Advances in Neural Information Processing Systems*, 37: 140589–140631, 2024.

Rakshitha Godahewa, Christoph Bergmeir, Geoffrey I Webb, Rob J Hyndman, and Pablo Montero-Manso. Monash time series forecasting archive.

Mononito Goswami, Konrad Szafer, Arjun Choudhry, Yifu Cai, Shuo Li, and Artur Dubrawski. Moment: A family of open time-series foundation models. *arXiv preprint arXiv:2402.03885*, 2024.

Shi Bin Hoo, Samuel Müller, David Salinas, and Frank Hutter. From tables to time: How tabpfn-v2 outperforms specialized time series forecasting models. *arXiv preprint arXiv:2501.02945*, 2025.

Alexis Huet, Jose Manuel Navarro, and Dario Rossi. Local evaluation of time series anomaly detection algorithms. In *Proceedings of the 28th ACM SIGKDD Conference on Knowledge Discovery and Data Mining*, pp. 635–645, 2022.

Deepak A Kaji, John R Zech, Jun S Kim, Samuel K Cho, Neha S Dangayach, Anthony B Costa, and Eric K Oermann. An attention based deep learning model of clinical events in the intensive care unit. *PloS one*, 14(2):e0211057, 2019.

Tian Lan, Yifei Gao, Yimeng Lu, and Chen Zhang. Cicada: Cross-domain interpretable coding for anomaly detection and adaptation in multivariate time series. *arXiv preprint arXiv:2505.00415*, 2025.

Fei Tony Liu, Kai Ming Ting, and Zhi-Hua Zhou. Isolation forest. In *2008 eighth ieee international conference on data mining*, pp. 413–422. IEEE, 2008.

Qinghua Liu and John Paparrizos. The elephant in the room: Towards a reliable time-series anomaly detection benchmark. *Advances in Neural Information Processing Systems*, 37:108231–108261, 2024.

Youngeun Nam, Susik Yoon, Yooju Shin, Minyoung Bae, Hwanjun Song, Jae-Gil Lee, and Byung Suk Lee. Breaking the time-frequency granularity discrepancy in time-series anomaly detection. In *Proceedings of the ACM Web Conference 2024*, pp. 4204–4215, 2024.

Yuqi Nie, Nam H Nguyen, Phanwadee Sinthong, and Jayant Kalagnanam. A time series is worth 64 words: Long-term forecasting with transformers. *arXiv preprint arXiv:2211.14730*, 2022.

John Paparrizos, Paul Boniol, Themis Palpanas, Ruey S Tsay, Aaron Elmore, and Michael J Franklin. Volume under the surface: a new accuracy evaluation measure for time-series anomaly detection. *Proceedings of the VLDB Endowment*, 15(11):2774–2787, 2022.

Hansheng Ren, Bixiong Xu, Yujing Wang, Chao Yi, Congrui Huang, Xiaoyu Kou, Tony Xing, Mao Yang, Jie Tong, and Qi Zhang. Time-series anomaly detection service at microsoft. In *Proceedings of the 25th ACM SIGKDD international conference on knowledge discovery & data mining*, pp. 3009–3017, 2019.

M Saquib Sarfraz, Mei-Yen Chen, Lukas Layer, Kunyu Peng, and Marios Koulakis. Position: Quo vadis, unsupervised time series anomaly detection? In *International Conference on Machine Learning*, pp. 43461–43476. PMLR, 2024.

Lifeng Shen, Zhuocong Li, and James Kwok. Timeseries anomaly detection using temporal hierarchical one-class network. *Advances in neural information processing systems*, 33:13016–13026, 2020.

Qichao Shentu, Beibu Li, Kai Zhao, Yang Shu, Zhongwen Rao, Lujia Pan, Bin Yang, and Chenjuan Guo. Towards a general time series anomaly detector with adaptive bottlenecks and dual adversarial decoders. *arXiv preprint arXiv:2405.15273*, 2024.

Xiaoming Shi, Shiyu Wang, Yuqi Nie, Dianqi Li, Zhou Ye, Qingsong Wen, and Ming Jin. Time-moe: Billion-scale time series foundation models with mixture of experts. *arXiv preprint arXiv:2409.16040*, 2024.

Ya Su, Youjian Zhao, Chenhao Niu, Rong Liu, Wei Sun, and Dan Pei. Robust anomaly detection for multivariate time series through stochastic recurrent neural network. In *Proceedings of the 25th ACM SIGKDD international conference on knowledge discovery & data mining*, pp. 2828–2837, 2019.

Ege Onur Taga, Muhammed Emrullah Ildiz, and Samet Oymak. Timepfn: Effective multivariate time series forecasting with synthetic data. In *Proceedings of the AAAI Conference on Artificial Intelligence*, volume 39, pp. 20761–20769, 2025.

Shreshth Tuli, Giuliano Casale, and Nicholas R Jennings. Tranad: deep transformer networks for anomaly detection in multivariate time series data. *Proceedings of the VLDB Endowment*, 15(6):1201–1214, 2022.

Ashish Vaswani, Noam Shazeer, Niki Parmar, Jakob Uszkoreit, Llion Jones, Aidan N Gomez, Łukasz Kaiser, and Illia Polosukhin. Attention is all you need. *Advances in neural information processing systems*, 30, 2017.

Garrett Wilson, Janardhan Rao Doppa, and Diane J Cook. Calda: Improving multi-source time series domain adaptation with contrastive adversarial learning. *IEEE transactions on pattern analysis and machine intelligence*, 45(12):14208–14221, 2023.

Gerald Woo, Chenghao Liu, Akshat Kumar, Caiming Xiong, Silvio Savarese, and Doyen Sahoo. Unified training of universal time series forecasting transformers. 2024.

Shifeng Xie, Vasilii Feofanov, Marius Alonso, Ambroise Odonnat, Jianfeng Zhang, Themis Palpanas, and Ievgen Redko. Cauker: classification time series foundation models can be pretrained on synthetic data only. *arXiv preprint arXiv:2508.02879*, 2025.

Zhe Xie, Zeyan Li, Xiao He, Longlong Xu, Xidao Wen, Tieying Zhang, Jianjun Chen, Rui Shi, and Dan Pei. Chatts: Aligning time series with llms via synthetic data for enhanced understanding and reasoning. *arXiv preprint arXiv:2412.03104*, 2024.

Jiehui Xu, Haixu Wu, Jianmin Wang, and Mingsheng Long. Anomaly transformer: Time series anomaly detection with association discrepancy. *arXiv preprint arXiv:2110.02642*, 2021.

Yiyuan Yang, Chaoli Zhang, Tian Zhou, Qingsong Wen, and Liang Sun. Dcdetector: Dual attention contrastive representation learning for time series anomaly detection. In *Proceedings of the 29th ACM SIGKDD conference on knowledge discovery and data mining*, pp. 3033–3045, 2023.

Zahra Zamanzadeh Darban, Geoffrey I Webb, Shirui Pan, Charu Aggarwal, and Mahsa Salehi. Deep learning for time series anomaly detection: A survey. *ACM Computing Surveys*, 57(1):1–42, 2024.

Chuxu Zhang, Dongjin Song, Yuncong Chen, Xinyang Feng, Cristian Lumezanu, Wei Cheng, Jingchao Ni, Bo Zong, Haifeng Chen, and Nitesh V Chawla. A deep neural network for unsupervised anomaly detection and diagnosis in multivariate time series data. In *Proceedings of the AAAI conference on artificial intelligence*, volume 33, pp. 1409–1416, 2019.

A USE OF LLMS

In preparing our manuscript, we used large language models (LLMs) only to aid or polish the writing. Their use was restricted to improving grammar, readability, and style, without contributing to the methodology, theoretical results, algorithmic implementation, or experimental outcomes. The involvement of LLMs does not affect the reproducibility of our findings.

B Related Work

State-of-the-art TSAD algorithm Traditional unsupervised TSAD operates by training models on domain-specific normal data to identify deviations in unseen test sets. Within this paradigm, two primary approaches have been dominant. Reconstruction-based methods identify anomalies by quantifying the error when attempting to rebuild an input signal, with higher errors indicating anomalous behavior (Audibert et al., 2020; Su et al., 2019; Zhang et al., 2019; Tuli et al., 2022; Nam et al., 2024). In parallel, contrastive-based methods learn discriminative representations by maximizing the distinction between normal and anomalous patterns or distributions (Xu et al., 2021; Yang et al., 2023; Shen et al., 2020; Darban et al., 2025; Lan et al., 2025; Wilson et al., 2023). However, the reliance of these methods on in-domain normal data presents a fundamental barrier to generalization, leading to significant performance degradation in zero-shot scenarios where the model encounters data from new, unseen domains. While the recent emergence of foundation models aims to overcome this transferability issue, the predominant architecture remains anchored in the reconstruction-based framework (Shentu et al., 2024; Gao et al., 2024; Goswami et al., 2024), which suffers from **objective dismatch**. We are the first to develop a foundation model for zero-shot TSAD built upon the principle of relative contextual discrimination, thereby circumventing the limitations of reconstruction-based approaches in zero-shot TSAD.

Synthetic dataset for Time series analysis The paradigm of leveraging synthetic data for pre-training time series models has been extensively validated, particularly in the domain of forecasting, where it has led to significant performance gains across various benchmarks (Xie et al., 2025; Cai et al., 2024; Dooley et al., 2023; Hoo et al., 2025; Taga et al., 2025; Bhethanabhotla et al., 2024). Following this trend, several foundation models for general time series analysis have been successfully trained on a hybrid corpus of real-world and synthetic data to enhance their generalization capabilities (Ansari et al., 2024; Das et al., 2024; Shi et al., 2024; Goswami et al., 2024). In contrast, the application of purely synthetic data for TSAD remains substantially less explored. Existing efforts in this area have primarily focused on data augmentation, where artificial anomalies are injected into real-world time series to enrich the training set (Shentu et al., 2024; Darban et al., 2025). While effective, these methods are still fundamentally dependent on the availability and diversity of the underlying real data. Other studies have discussed the generation of entirely synthetic anomalous time series but have not applied this data to the end-to-end training of a dedicated TSAD model (Cai et al., 2024; Xie et al., 2024). To the best of our knowledge, this work is the first to propose and successfully implement a pre-training framework for a foundation model dedicated to TSAD that relies exclusively on a large-scale, fully synthetic dataset.

C Data Generation

Our synthetic data generation framework is designed as a curriculum to instill a universal understanding of temporal dynamics and causality in a model. The four-stage process is meticulously designed to first build a complex, predictable "normal" context (Stages 1-2) and then introduce meaningful, context-violating anomalies (Stage 3). Finally, we generate causally-aware ground-truth labels that teach the model to link an anomaly's root cause to its downstream effects (Stage 4), preparing it for zero-shot detection on unseen systems.

Stage 1: Synthesizing the "Normal" Univariate Context Every time series, whether it stands alone or is a component in a multivariate system, begins as a univariate baseline signal, $x_{\text{base}}(t)$. This signal is constructed as an additive composite of trend, seasonal, and noise components:

$$x_{\text{base}}(t) = T(t) + S(t) + \varepsilon(t), \quad t = 0, 1, \ldots, n-1.$$

Sequence length. we sample n from 100 to 10000 to match variable-length sequences.

Trend $T(t)$**.** We mix deterministic and stochastic trends: $T_{\text{det}}(t)$ and $T_{\text{stoc}}(t)$. Set $T(t) = (1-\rho_T)\,T_{\text{det}}(t) + \rho_T\,T_{\text{stoc}}(t)$ with $\rho_T \in [0,1]$. The detailed construction of trend is shown in Appendix C.2

Seasonality $S(t)$**.** A mixture of K periodic atoms:

$$S(t) = \sum_{k=1}^{K} A_k\, w_k(2\pi f_k t + \varphi_k; \theta_k)\,,$$

where w_k is selected from a library (sinusoid, square/triangle wave, wavelet atom), with amplitude $A_k > 0$, frequency f_k, phase φ_k, and shape parameters θ_k (e.g., duty cycle for square, mother/scale for wavelets). Frequencies may be harmonic $f_k = m_k f_0$ or incommensurate. The detailed construction of seasonality is shown in Appendix C.3

Noise $\varepsilon(t)$**.** Zero-mean noise with optional piecewise volatility:

$$\varepsilon(t) \sim \mathcal{N}\big(0,\, \sigma^2(t)\big), \qquad \sigma(t) = \sigma_0 \prod_{r=1}^{R} \big(1 + \upsilon_r\, \mathbf{1}_{[a_r, b_r)}(t)\big),$$

allowing volatility bursts over windows $[a_r, b_r)$. This captures heteroskedastic segments..

Stage 2: Weaving the Multivariate Causal Context via a Discretized ODE System This stage creates a multivariate system with clear causal dependencies. We first conceptualize continuous-time causal dynamics (ODE), then discretize to an AutoRegressive with eXogenous inputs (ARX) model via Euler.

1. **Generate a Causal Structure (DAG):** Sample a directed acyclic graph $G = (V, E)$ over N nodes by first drawing an Erdős–Rényi graph and then orienting edges along a random topological order to avoid cycles. Edge presence is controlled by $p_{\text{edge}} \in (0,1)$. An edge $(j,i) \in E$ means series j causally influences i.
2. **Define the Continuous-Time Causal Dynamics (ODE Model):** We model the evolution of the **causal influence** on each node, $z_i(t)$, as a first-order linear ODE. This equation describes how the influence on node i changes over time based on its own internal state and forcing from its parent nodes $P(i)$:
$$\frac{dz_i(t)}{dt} = -\gamma_i z_i(t) + \sum_{j \in P(i)} \beta_{ij} x_j(t - \tau_{ij}) + C_i$$
Here, $-\gamma_i z_i(t)$ represents an internal decay term, the sum represents the forcing from parent nodes x_j, and C_i is a constant bias.
3. **Discretize to an ARX Model for Implementation:** With Euler and $\Delta t = 1$, the discrete ARX is
$$z_i[t] = a_i z_i[t-1] + \sum_{j \in P(i)} b_{ij} x_j[t - \ell_{ij}] + c_i, \quad |a_i| \le 0.8,$$
where $a_i = 1 - \gamma_i$ encodes decay stability, delays $\ell_{ij} \in \{0, \dots, \ell_{\max}\}$, and b_{ij} are exogenous gains. We sample $a_i \sim \mathcal{U}[-0.8, 0.8]$, $\ell_{ij} \sim \mathcal{U}\{0, \dots, \ell_{\max}\}$, and $b_{ij} \sim \mathcal{N}(0, \sigma_b^2)$ (variance scaled by in-degree).
4. **Mix the Signals:** The observed node mixes baseline with causal channel:
$$x_i[t] = (1 - \alpha_i)\, x_{\text{base},i}(t) + \alpha_i\, z_i[t], \quad \alpha_i \in [0,1].$$
In vector form ($x[t], z[t] \in \mathbb{R}^N$),
$$z[t] = A\, z[t-1] + \sum_{\delta=0}^{\ell_{\max}} B^{(\delta)} x[t-\delta] + c, \quad x[t] = (I - A')\, x_{\text{base}}(t) + A'\, z[t],$$
where $A = \operatorname{diag}(a_i)$, $A' = \operatorname{diag}(\alpha_i)$, and $B^{(\delta)}$ encodes lagged influences.

This process, performed sequentially according to the topological sort, creates a system where a change in a parent node will naturally propagate to its child nodes after a specified delay.

Stage 3: Principled Anomaly Injection: Simulating Causal and Contextual Complexity Our primary contribution in data generation lies in a synthetic framework designed to address critical gaps in existing anomaly detection benchmarks, namely the lack of causal realism and contextual complexity. To achieve this, our methodology introduces a novel causal framework for generating anomalies based on two distinct, complementary philosophies:

- **Endogenous Anomaly (Internal System Failure):** This strategy simulates how a single root-cause anomaly propagates through an interconnected system. An anomaly is introduced into the baseline series of a parent node *before* causal mixing. Its effects are then passed to descendant nodes based on the ARX model, creating a realistic cascade of causally-linked anomalous events.
- **Exogenous Anomaly (External Shock):** This mirrors more conventional techniques, modeling an external event impacting an otherwise normal system. The normal multivariate system is fully generated first, and then a segment of a single series is overwritten with an anomalous template.

In addition to causal dynamics, we move beyond simple point anomalies by creating a rich taxonomy of contextual anomalies designed to violate specific, established patterns within the data. These include:

- **Local/Change Anomalies:** Additive templates, $\Delta(t)$, applied over a window, representing events like a sudden sensor glitch (**Spike**), a component failure shifting its baseline (**Level Shift**), or mechanical vibrations (**Shake**).
$$x'_{\text{anom}}(t) = x_{\text{norm}}(t) + \Delta(t) \quad \text{for } t \in [t_s, t_e)$$
- **Seasonal Anomalies:** The normal seasonal component $S(t)$ is replaced with an altered version $S'(t)$. They simulate systemic issues like a machine operating at the wrong speed (**Frequency Change**) or a process desynchronization (**Phase Shift**).
$$x'_{\text{anom}}(t) = T(t) + S'(t) + \varepsilon(t) \quad \text{for } t \in [t_s, t_e)$$

In contrast to methods that inject isolated anomalies into independent time series, our dual-pronged approach provides a more challenging and realistic benchmark. By generating complex scenarios with both contextual violations and causal propagation, our dataset enables a more robust evaluation of a model's ability to understand system-wide dynamics. Details of constructing different abnormal types in the C.4

C.1 Hyperparameters and Sampling Mappings

To make the generation process transparent yet non-programmatic, we group hyperparameters into: dataset-level controls (Table 3); attribute families and their sampling weights (Table 4); multivariate graph and causal dynamics (Table 5).

C.2 Trend Types and Formal Definitions

We instantiate the trend component $T(t)$ using five archetypes aligned with the generator configuration. Let $t \in \{0, \ldots, n-1\}$.

Increase / Decrease / Keep steady. We use an affine model
$$T(t) = k_0 + k_1 t,$$
with constraints: *increase* uses $k_1 > 0$, *decrease* uses $k_1 < 0$, and *keep steady* uses $k_1 = 0$ (constant baseline).

Table 3: Dataset-level generation controls and intended effects.

Name	Typical range / rule	Applies to	Intended effect
Number of samples	positive integer	whole dataset	Total number of generated sequences.
Sequence length	uniformly in $\{100, \ldots, 10000\}$	per sample	Time horizon of each sequence.
Anomalous-sample ratio	real in $[0, 1]$	per sample	Probability a sample contains anomalies.
Multivariate flag	{True, False}	per sample	Whether to generate multi-channel series.
Number of features	fixed or uniformly in $\{2, \ldots, 50\}$	multivariate only	Channel count when multivariate.
Random seed (optional)	user-provided integer	whole run	Reproducibility of the random draws.

Table 4: Attribute categories, options, and relative probability.

Category	Options	Probability
Seasonality type	no periodic fluctuation	0.3
	sine	0.3
	square	0.05
	triangle	0.05
	wavelet	0.3
Trend type	decrease	0.2
	increase	0.2
	keep steady	0.2
	multiple	0.3
	ARIMA	0.1
Frequency regime	high frequency	0.5
	low frequency	0.5
Noise level	almost no noise	0.25
	low	0.25
	moderate	0.25
	high	0.25

Multiple (piecewise trend). To capture mixed regimes, we allow P change-points at integer knots $0 < \tau_1 < \cdots < \tau_P < n$ and define a piecewise-linear trend with slope updates:

$$T(t) = k_0 + k_1 t + \sum_{p=1}^{P} \delta_p \left[t \geq \tau_p\right] (t - \tau_p)_+,$$

where $(u)_+ = \max\{u, 0\}$ and δ_p adjusts slope after each τ_p. This matches the additive hinge construction used in Stage 1.

ARIMA (stochastic trend). For stochastic trends we use a differenced ARMA process. Let ∇^d be the d-th difference operator. A general ARIMA(p, d, q) satisfies

$$\phi(B)\, \nabla^d T(t) = \theta(B)\, \varepsilon_T(t), \qquad \varepsilon_T(t) \sim \mathcal{N}(0, \sigma_T^2),$$

with backshift B, AR polynomial $\phi(B) = 1 - \sum_{i=1}^{p} \phi_i B^i$, and MA polynomial $\theta(B) = 1 + \sum_{j=1}^{q} \theta_j B^j$. In practice we use small orders (e.g., $p, q \leq 2$) and modest variance.

C.3 Seasonality Types and Formal Definitions

We support five seasonal archetypes. Let the base period be $P > 0$ (in samples), frequency $f = 1/P$, amplitude $A > 0$, and phase $\varphi \in [0, 2\pi)$.

No periodic fluctuation. No seasonality is present:

$$S(t) = 0.$$

Table 5: Multivariate and causal-dynamics hyperparameters and intended roles.

Name	Typical range / rule	Applies to	Intended role
Number of nodes	Uniformly in 1 to 50	system graph	Dimensionality of the multivariate system.
Number of edges	roughly linear in nodes (acyclic)	system graph	Connectivity while preserving acyclicity.
Parent lags	nonnegative integers up to a small fraction of length	per edge	Causal delays between channels.
ARX autoregression a_i	real in $[-0.8, 0.8]$	per node	Decay/stability of latent causal influence.
ARX exogenous gains b_{ij}	zero-mean with finite variance	per edge	Strength of parent-to-child coupling.
ARX bias c_i	bounded real interval	per node	Baseline offset in causal channel.
Mixing weight α_i	real in $[0, 1]$	per node	Balance between baseline and causal channel.

Sin periodic fluctuation. A sinusoidal component:

$$S(t) = A\,\sin\big(2\pi f t + \varphi\big).$$

Square periodic fluctuation. A rectangular wave with duty cycle $d \in (0, 1)$:

$$S(t) = A\,\operatorname{sgn}\big(\sin(2\pi f t + \varphi)\big),$$

or equivalently by its Fourier series $S(t) = \frac{4A}{\pi} \sum_{m\,\text{odd}} m^{-1} \sin(2\pi m f t + \varphi)$; duty-cycle variants modulate on/off durations per period.

Triangle periodic fluctuation. A symmetric triangle wave of period P:

$$S(t) = \frac{8A}{\pi^2} \sum_{m\,\text{odd}} \frac{(-1)^{(m-1)/2}}{m^2} \sin(2\pi m f t + \varphi),$$

equivalently realizable as a piecewise-linear ramp that rises and falls within each period.

Wavelet periodic fluctuation. A sum of localized atoms (e.g., `db`, `sym`, `coif`, `haar`, `bior`, `dmey` families):

$$S(t) = \sum_{\ell=1}^{L} A_\ell\, \psi_\ell\!\left(\frac{t - \tau_\ell}{s_\ell}\right), \qquad A_\ell \in \mathbb{R},\ s_\ell > 0,\ \tau_\ell \in \mathbb{R}.$$

C.4 A Taxonomy of Synthetic Anomaly Archetypes

Following the high-level description, we now provide complete, self-contained definitions and formulas for each anomaly type supported by our generator. We divide them into two families: Local/Change Anomalies (abrupt, windowed changes) and Seasonal Anomalies (contextual violations of periodic structure). We avoid shorthand; every symbol is explicitly defined. A comprehensive summary of all anomaly archetypes with intents and formal definitions is provided in Table 6.

Notation and primitives. We use discrete time index $t \in \{0, 1, \ldots, n-1\}$. The normal (anomaly-free) series is denoted by $x_{\text{norm}}(t)$. An anomaly acts on a closed-open window $[t_s, t_e)$ with integers $0 \le t_s < t_e \le n$. The indicator function is

$$\mathbf{1}_{[t_s,t_e)}(t) = \begin{cases} 1, & t_s \le t < t_e, \\ 0, & \text{otherwise.} \end{cases}$$

The Heaviside step function at integer times is $H(t; t_0) = \mathbf{1}_{[t_0,\infty)}(t)$. For any scalar u, the logistic sigmoid is $\sigma(u) = \frac{1}{1+e^{-u}}$. For a rectangular window we use $h(t; t_s, t_e) = \mathbf{1}_{[t_s,t_e)}(t)$. All amplitudes $A, B, \{A_m\}$ are real scalars; all durations and lags (e.g., w, τ_r, τ_f, d) are positive integers unless otherwise stated.

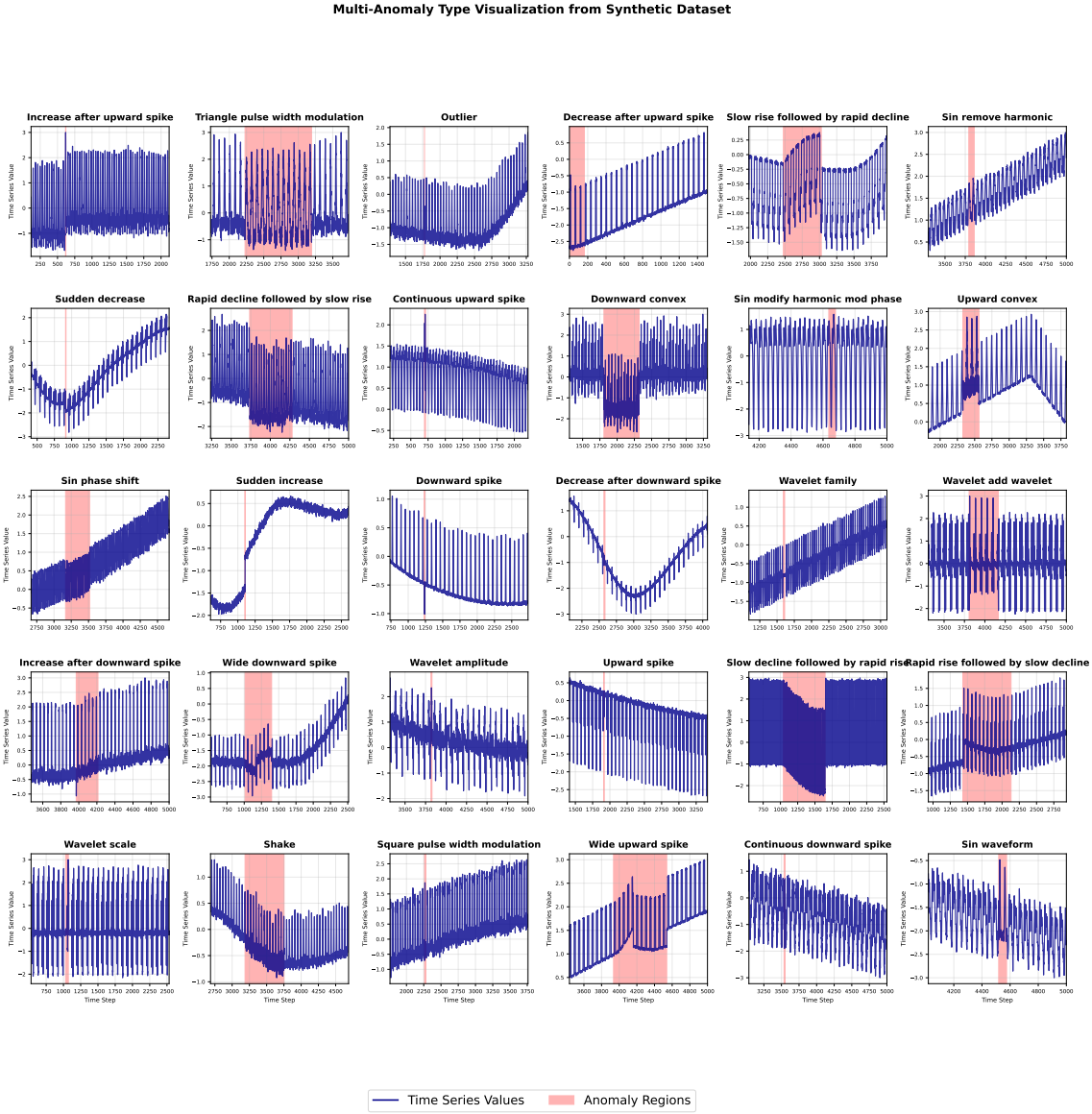
Multi-Anomaly Type Visualization from Synthetic Dataset
Increase after upward spike
Triangle pulse width modulation
Outlier
Decrease after upward spike
Slow rise followed by rapid decline
Sin remove harmonic
Sudden decrease
Rapid decline followed by slow rise
Continuous upward spike
Downward convex
Sin modify harmonic mod phase
Upward convex
Sin phase shift
Sudden increase
Downward spike
Decrease after downward spike
Wavelet family
Wavelet add wavelet
Increase after downward spike
Wide downward spike
Wavelet amplitude
Upward spike
Slow decline followed by rapid rise
Rapid rise followed by slow decline
Wavelet scale
Shake
Square pulse width modulation
Wide upward spike
Continuous downward spike
Sin waveform
Time Series Value
Time Step
Time Series Values
Anomaly Regions

C.4.1 LOCAL/CHANGE ANOMALIES

All local anomalies are applied additively within a window using a template $\Delta(t)$:

$$x'_{\text{anom}}(t) = x_{\text{norm}}(t) + \Delta(t)\,\mathbf{1}_{[t_s,t_e)}(t), \quad t = 0, 1, \ldots, n-1.$$

Spikes and bursts

- **Upward spike** (a single sharp positive glitch). Parameters: center time $t_0 \in [t_s, t_e)$, half-width $w \in \mathbb{N}^+$, amplitude $A > 0$. Define

$$\Delta(t) = A\,\max\!\left(1 - \frac{|t - t_0|}{w},\, 0\right), \quad t \in \mathbb{Z}.$$

- **Downward spike** (a single sharp negative glitch). Same parameters as above with negative amplitude:

$$\Delta(t) = -A\,\max\!\left(1 - \frac{|t - t_0|}{w},\, 0\right).$$

- **Continuous upward spikes** (a burst of multiple positive spikes). Parameters: spike count $M \in \mathbb{N}^+$, centers spaced by stride $d \in \mathbb{N}^+$, per-spike amplitudes $A_m > 0$, per-spike widths $w_m \in \mathbb{N}^+$. Define

$$\Delta(t) = \sum_{m=0}^{M-1} A_m\,\max\!\left(1 - \frac{|t - (t_0 + md)|}{w_m},\, 0\right).$$

- **Continuous downward spikes** (a burst of negative spikes). Use

$$\Delta(t) = \sum_{m=0}^{M-1} (-A_m)\,\max\!\left(1 - \frac{|t - (t_0 + md)|}{w_m},\, 0\right).$$

- **Wide upward spike** (longer rise, short plateau, and fall). Parameters: rise length $\tau_r \in \mathbb{N}^+$, fall length $\tau_f \in \mathbb{N}^+$, amplitude $A > 0$. Define

$$\Delta(t) = \begin{cases} A\,\frac{t - t_s}{\tau_r}, & t \in [t_s, t_s + \tau_r), \\ A, & t \in [t_s + \tau_r, t_e - \tau_f), \\ A\left(1 - \frac{t - (t_e - \tau_f)}{\tau_f}\right), & t \in [t_e - \tau_f, t_e), \\ 0, & \text{else.} \end{cases}$$

- **Wide downward spike** (longer fall then recovery). Use the same piecewise definition with amplitude $-A$.
- **Outlier** (single-point shock). Parameters: position $t_0 \in [t_s, t_e)$, amplitude $A \in \mathbb{R}$. Define the Kronecker impulse

$$\Delta(t) = \begin{cases} A, & t = t_0, \\ 0, & t \neq t_0. \end{cases}$$

Level shifts and plateaus

- **Sudden increase** (permanent level up-shift). Parameters: slope parameter $\kappa > 0$, amplitude $A > 0$, change time $t_0 \in [t_s, t_e)$. Define

$$\Delta(t) = A\,\sigma\big(\kappa(t - t_0)\big), \quad \sigma(u) = \frac{1}{1 + e^{-u}}.$$

- **Sudden decrease** (permanent level down-shift). Use

$$\Delta(t) = -A\,\sigma\big(\kappa(t - t_0)\big).$$

- **Convex/Concave plateau** (temporary level change using a raised-cosine window). Parameters: window $[t_s, t_e)$, amplitude $A > 0$, sign $s \in \{+1, -1\}$ (convex when $s = +1$, concave when $s = -1$). Define

$$\Delta(t) = s\,A\,\tfrac{1}{2}\left(1 - \cos\frac{\pi(t - t_s)}{t_e - t_s}\right)\mathbf{1}_{[t_s,t_e)}(t).$$

Asymmetric transients

- **Rapid rise followed by slow decline**. Parameters: rise time constant $\tau_r \in \mathbb{N}^+$, fall time constant $\tau_f \in \mathbb{N}^+$, peak time $t_p \in [t_s, t_e]$, amplitude $A > 0$. Define

$$\Delta(t) = A\Big(1 - e^{-\frac{t-t_s}{\tau_r}}\Big)\mathbf{1}_{[t_s,t_p)}(t) + A\,e^{-\frac{t-t_p}{\tau_f}}\mathbf{1}_{[t_p,t_e)}(t), \quad \tau_r \ll \tau_f.$$

- **Slow rise followed by rapid decline**. Use the same definition with $\tau_r \gg \tau_f$.
- **Rapid decline followed by slow rise**. Use the above definition with amplitude $-A$ and swap rise/fall roles accordingly.
- **Slow decline followed by rapid rise**. Use the rapid rise–slow decline formula with amplitude $-A$ and $\tau_r \gg \tau_f$.

Spike + level interaction

- **Decrease after upward spike**. Parameters: spike template $\Delta_{\text{spk}}(t)$ (e.g., the triangular spike above), post-spike shift magnitude $B > 0$, shift start $t_1 \geq t_s$. Define

$$\Delta(t) = \Delta_{\text{spk}}(t) - B\,H(t; t_1), \quad H(t; t_1) = \mathbf{1}_{[t_1,\infty)}(t).$$

- **Increase after downward spike**. Using a negative spike template $\Delta_{\text{nspk}}(t)$ and a positive shift $B > 0$:

$$\Delta(t) = \Delta_{\text{nspk}}(t) + B\,H(t; t_1).$$

- **Increase after upward spike**. Use

$$\Delta(t) = \Delta_{\text{spk}}(t) + B\,H(t; t_1).$$

- **Decrease after downward spike**. Use

$$\Delta(t) = \Delta_{\text{nspk}}(t) - B\,H(t; t_1).$$

High-frequency burst

- **Shake** (localized high-frequency vibration). Parameters: carrier frequency $f_h \in \mathbb{R}_{>0}$ in cycles per sample, phase $\varphi \in [0, 2\pi)$, amplitude $A > 0$. With a rectangular window $h(t; t_s, t_e)$,

$$\Delta(t) = A\,h(t; t_s, t_e)\,\sin(2\pi f_h t + \varphi).$$

C.4.2 SEASONAL ANOMALIES

Seasonal anomalies are implemented by replacing the seasonal component $S(t)$ with a modified component $S'(t)$ strictly within the window $[t_s, t_e)$, while leaving the rest unchanged:

$$x'_{\text{anom}}(t) = \begin{cases} T(t) + S'(t) + \varepsilon(t), & t_s \le t < t_e, \\ T(t) + S(t) + \varepsilon(t), & \text{otherwise.} \end{cases}$$

Universal transforms (any waveform)

- **Waveform inversion** (polarity flip). For $t \in [t_s, t_e)$, set $S'(t) = -S(t)$.
- **Amplitude scaling**. For $t \in [t_s, t_e)$, set $S'(t) = r\,S(t)$ with scaling factor $r > 0$.
- **Frequency change**. Let the original period be $P > 0$ and frequency $f = 1/P$. Choose a period multiplier $\rho > 0$ and set the new period $P' = \rho P$ and frequency $f' = 1/P'$. For a sinusoid $S(t) = A\sin(2\pi f t + \varphi)$, define $S'(t) = A\sin(2\pi f' t + \varphi)$ for $t \in [t_s, t_e)$.
- **Noise injection**. For $t \in [t_s, t_e)$, set $S'(t) = S(t) + \eta(t)$ with i.i.d. Gaussian noise $\eta(t) \sim \mathcal{N}(0, \sigma_S^2)$.
- **Waveform change from sine to square/triangle**. If $S(t)$ is sinusoidal with amplitude A and period P, replace it by a square/triangle waveform $w_{\text{new}}(t; A, P, \theta)$ of the same amplitude and period (with shape parameters θ) for $t \in [t_s, t_e)$.

Sinusoidal-specific (harmonics and phase) Let a sinusoidal seasonal component be represented by a finite harmonic sum

$$S(t) = \sum_{n=1}^{N} A_n \sin\big(2\pi n f\, t + \varphi_n\big),$$

and optionally include amplitude modulation for each harmonic via

$$A_n(t) = \frac{A_n}{n}\left(1 + d_n \sin(\omega_m t + \psi_n)\right), \quad d_n \in [0, 1),\ \omega_m > 0,\ \psi_n \in [0, 2\pi).$$

- **Phase shift**. For $t \in [t_s, t_e)$, update all phases by a fixed shift $\Delta\varphi \in (0, 2\pi)$: $\varphi_n \mapsto \varphi_n + \Delta\varphi$.
- **Add harmonic**. For $t \in [t_s, t_e)$, add a new harmonic of order $m \in \mathbb{N}^+$: $S'(t) = S(t) + A_h \sin(2\pi m f\, t + \varphi_h)$ with amplitude $A_h > 0$ and phase $\varphi_h \in [0, 2\pi)$.
- **Remove harmonic**. For $t \in [t_s, t_e)$, remove one existing harmonic index $n^* \in \{1, \ldots, N\}$ from the sum, keeping the others unchanged.
- **Modify harmonic phase**. For $t \in [t_s, t_e)$, choose one index n^* and set $\varphi_{n^*} \mapsto \varphi'_{n^*}$ such that $|\varphi'_{n^*} - \varphi_{n^*}| \ge \delta$ for a given threshold $\delta > 0$.
- **Modify amplitude-modulation depth**. For $t \in [t_s, t_e)$, choose index n^* and set $d_{n^*} \mapsto d'_{n^*}$ within $[0, 1)$.
- **Modify modulation frequency**. For $t \in [t_s, t_e)$, update $\omega_m \mapsto \omega'_m$ with $\omega'_m > 0$.
- **Modify modulation phase**. For $t \in [t_s, t_e)$, choose index n^* and set $\psi_{n^*} \mapsto \psi'_{n^*}$.

Square/Triangle-specific (pulse geometry) For a square or triangle waveform with period $P > 0$, define the duty cycle $d \in (0, 1)$ as the fraction of each period the waveform is at its high level, and define a cycle start parameter $\delta \in [0, 1)$ that shifts the waveform phase relative to each period.

- **Pulse shift**. For $t \in [t_s, t_e)$, apply a phase shift $\Delta \in (-1, 1)$ cycles: $\delta \mapsto (\delta + \Delta) \bmod 1$.

- **Pulse width modulation**. For $t \in [t_s, t_e)$, scale the duty cycle by a factor $\lambda > 0$: $d \mapsto d' = \min\{1, \max\{0, \lambda d\}\}$.

Wavelet-based (atoms and families) Let a wavelet-based seasonal component be represented as a finite sum of atoms

$$S(t) = \sum_{\ell=1}^{L} A_\ell \, \psi_\ell\left(\frac{t - \tau_\ell}{s_\ell}\right), \quad A_\ell \in \mathbb{R},\ s_\ell > 0,\ \tau_\ell \in \mathbb{R}.$$

- **Family change**. For $t \in [t_s, t_e)$, replace each mother wavelet ψ_ℓ taken from a family $\mathcal{F}$ by a corresponding wavelet $\tilde{\psi}_\ell$ from a different family $\tilde{\mathcal{F}}$ while keeping $A_\ell, s_\ell, \tau_\ell$ unchanged.
- **Scale change**. For $t \in [t_s, t_e)$, update scales by a factor $\lambda > 0$: $s_\ell \mapsto s'_\ell = \lambda s_\ell$ for selected indices.
- **Shift change**. For $t \in [t_s, t_e)$, update translations by $\tau_\ell \mapsto \tau'_\ell = \tau_\ell + \Delta_{\tau,\ell}$.
- **Amplitude change**. For $t \in [t_s, t_e)$, rescale coefficients by $A_\ell \mapsto r_\ell \, A_\ell$ with $r_\ell > 0$.
- **Add wavelet**. For $t \in [t_s, t_e)$, append a new atom $A_+ \, \psi_+\big(\frac{t-\tau_+}{s_+}\big)$ with specified parameters.
- **Remove wavelet**. For $t \in [t_s, t_e)$, remove one existing atom index from the sum.

Table 6: Summary of anomaly archetypes, intents, and formal definitions.

Family	Type	Intent (one sentence)	Formal definition (within $[t_s, t_e)$)
Local	Upward spike	A single sharp positive glitch	$\Delta(t) = A \max(1 - \lvert t - t_0\rvert / w, 0)$
	Downward spike	A single sharp negative glitch	$\Delta(t) = -A \max(1 - \lvert t - t_0\rvert / w, 0)$
	Continuous upward spikes	Rapid consecutive positive spikes	$\sum_{m=0}^{M-1} A_m \max(1 - \lvert t - (t_0 + md)\rvert / w_m, 0)$
	Continuous downward spikes	Rapid consecutive negative spikes	$\sum_{m=0}^{M-1} (-A_m) \max(1 - \lvert t - (t_0 + md)\rvert / w_m, 0)$
	Wide upward spike	Longer rise/plateau/fall pulse	piecewise linear rise/hold/fall with amplitude A
	Wide downward spike	Longer fall/plateau/rise pulse	piecewise linear with amplitude $-A$
	Outlier	Single-point shock	$\Delta(t) = A$ if $t = t_0$, else 0
	Sudden increase	Permanent upward level shift	$\Delta(t) = A\,\sigma(\kappa(t - t_0))$
	Sudden decrease	Permanent downward level shift	$\Delta(t) = -A\,\sigma(\kappa(t - t_0))$
	Convex/Concave plateau	Temporary level change	$sA\frac{1}{2}\big(1 - \cos(\pi(t - t_s)/(t_e - t_s))\big)$
	Rapid rise $\to$ slow decline	Fast excitation then slow decay	$A(1 - e^{-(t-t_s)/\tau_r})\mathbf{1}_{[t_s,t_p)} + Ae^{-(t-t_p)/\tau_f}\mathbf{1}_{[t_p,t_e)}$
	Slow rise $\to$ rapid decline	Slow excitation then fast decay	same as above with $\tau_r \gg \tau_f$
	Rapid decline $\to$ slow rise	Fast drop then slow recovery	negative-amplitude version of above
	Slow decline $\to$ rapid rise	Slow drop then fast recovery	negative-amplitude version of above
	Decrease after upward spike	Spike followed by downward shift	$\Delta_{\text{spk}}(t) - B\,H(t; t_1)$
	Increase after downward spike	Negative spike then upward shift	$\Delta_{\text{nspk}}(t) + B\,H(t; t_1)$
	Increase after upward spike	Spike followed by upward shift	$\Delta_{\text{spk}}(t) + B\,H(t; t_1)$
	Decrease after downward spike	Negative spike then downward shift	$\Delta_{\text{nspk}}(t) - B\,H(t; t_1)$
	Shake	Localized high-frequency vibration	$A\sin(2\pi f_h t + \varphi)$ within $[t_s, t_e)$
Seasonal	Waveform inversion	Polarity flip of seasonal component	$S'(t) = -S(t)$
	Amplitude scaling	Change seasonal magnitude	$S'(t) = r\,S(t)$
	Frequency change	Alter base period/frequency	$S'(t)$ with $P' = \rho P$ (e.g., $f' = 1/P'$)
	Noise injection	Add Gaussian noise to seasonality	$S'(t) = S(t) + \eta(t),\ \eta \sim \mathcal{N}(0, \sigma_S^2)$
	Waveform change (sin$\to$square/triangle)	Replace waveform family	$S'(t) = w_{\text{new}}(t; A, P, \theta)$
	Phase shift (sinusoid)	Global phase offset	$\varphi_n \mapsto \varphi_n + \Delta\varphi$
	Add harmonic (sinusoid)	Introduce new harmonic	$S'(t) = S(t) + A_h \sin(2\pi m f t + \varphi_h)$
	Remove harmonic (sinusoid)	Remove one harmonic	drop index n^* term in $\sum_n$
	Modify harmonic phase	Change one harmonic phase	$\varphi_{n^*} \mapsto \varphi'_{n^*}$
	Modify amp-mod depth	Change amplitude modulation depth	$d_{n^*} \mapsto d'_{n^*}$
	Modify modulation frequency	Change modulation frequency	$\omega_m \mapsto \omega'_m$
	Modify modulation phase	Change modulation phase	$\psi_{n^*} \mapsto \psi'_{n^*}$
	Pulse shift (square/triangle)	Shift cycle start	$\delta \mapsto (\delta + \Delta) \bmod 1$
	Pulse width modulation	Change duty cycle	$d \mapsto d' = \min\{1, \max\{0, \lambda d\}\}$
	Wavelet family change	Swap mother wavelet family	$\psi_\ell \in \mathcal{F} \to \tilde{\psi}_\ell \in \tilde{\mathcal{F}}$
	Wavelet scale change	Rescale atom width	$s_\ell \mapsto s'_\ell = \lambda s_\ell$
	Wavelet shift change	Shift atom translation	$\tau_\ell \mapsto \tau'_\ell$
	Wavelet amplitude change	Rescale atom amplitude	$A_\ell \mapsto r_\ell A_\ell$
	Add wavelet atom	Add new atom	append $(A_+, s_+, \tau_+, \psi_+)$
	Remove wavelet atom	Remove existing atom	delete one summand index

D DETAILS OF EXPERIMENTS

D.1 BENCHMARK DATASETS

Our evaluation uses a selection of datasets from one primary source, the TSB-AD benchmark by Liu & Paparrizos (2024).

- **Univariate Datasets**: We utilize a diverse collection of univariate datasets including IOPS, MGAB, NAB, NEK, Power, SED, TODS, UCR, and YAHOO.
- **Multivariate Datasets**: For multivariate anomaly detection, we use the SWaT, WADI, SMD, MSL, and PSM datasets. These are sourced from industrial control systems and spacecraft telemetry, presenting complex, multi-dimensional dependencies.

The specific characteristics of these datasets, including their domain, number of time series (TS), average length, and anomaly ratio, are summarized in Table 7 and Table 8.

Table 7: Univariate Datasets

Name	Domain	#TS	Avg Length	AR (%)
UCR	Misc.	228	67818.7	0.6
NAB	Web	28	5099.7	10.6
YAHOO	Web	259	1560.2	0.6
IOPS	Operations	17	72792.3	1.3
MGAB	Sensor	9	97777.8	0.2
SED	Energy	3	23332.3	4.1
TODS	Traffic	15	5000.0	6.3
NEK	Weather	9	1073.0	8.0
Power	Power Grid	1	35040.0	8.5

Table 8: Multivariate Datasets

Name	Domain	#TS	Avg Length	AR (%)
MSL	Space	16	3119.4	5.1
PSM	Sensor	1	217624.0	11.2
SMAP	Space	27	7855.9	2.9
SMD	Server	22	25466.4	3.8
SWaT	ICS	2	207457.5	12.7

D.2 BASELINES

Our study compares a range of baseline models, categorized into zero-shot and full-shot detectors, following the methodology from TSB-AD benchmark (Liu & Paparrizos, 2024) and the DADA (Shentu et al., 2024).

Zero-Shot Models These models are pre-trained on large-scale datasets and can be applied directly to new time series without fine-tuning.

- **DADA**: This model, from the paper by (Shentu et al., 2024), is a pre-trained general anomaly detector. We set the window size to 100.

- **TS-Pulse**: An IBM foundation model that uses a TSMixer architecture (Ekambaram et al., 2025). It is pre-trained on a massive corpus for multi-task applications, including anomaly detection. Following the suggestion from the paper, we set the window size with a length of 96.
- **MOMENT**: A foundation model that utilizes a patch-based pre-training strategy to learn rich representations from diverse time series data (Goswami et al., 2024). We use a window size of 64.
- **TimesFM**: A decoder-only transformer model from Google trained on a large time series corpus using a patching strategy, enabling strong zero-shot generalization (Das et al., 2024). We set the window size to 96.
- **Chronos**: A generative model that frames time series analysis as a language modeling task, using a transformer-based architecture to learn and predict time series values (Ansari et al., 2024). Its window size is 100.
- **Time MOE**: A decoder-only transformer model with a sparse Mixture-of-Experts (MoE) architecture. It is pre-trained on a large time series corpus for forecasting and multi-task learning (Shi et al., 2024). We set the window size to 96.

Full-Shot Models These models require training on the target dataset.

- **TranAD**: A transformer-based model that uses a reconstructive approach to detect anomalies by comparing original and reconstructed time series (Tuli et al., 2022). It is configured with a window size of 10.
- **USAD**: An autoencoder-based model that employs an adversarial training mechanism to enhance its reconstruction capability and anomaly detection (Audibert et al., 2020). We set the window size to 100.
- **OmniAnomaly**: A deep learning model that uses a Variational Autoencoder (VAE) with a Gated Recurrent Unit (GRU) to learn normal patterns and detect deviations (Su et al., 2019). The model is configured with a window size of 100.
- **LOF**: A traditional statistical method that measures the local deviation of a data point from its neighbors, identifying anomalies with lower local density (Breunig et al., 2000). For univariate datasets, we set n neighbors to 50, and for multivariate, we set n neighbors to 50 with metric as euclidean.
- **IForest**: An ensemble of Isolation Trees that isolates anomalies based on the number of random partitions required to separate them from the rest of the data (Liu et al., 2008). For univariate datasets, we set n estimators to 200, and for multivariate, we set n estimators to 25 and max features to 0.8.

D.3 Evaluation Metric Calculations

Our performance evaluation is conducted using four metrics: Affiliation F1 ($F1_A$), Temporal F1 ($F1_T$), Standard F1 ($F1$), and VUS-PR. We adopt a selection of metrics from the TSB-AD benchmark (Liu & Paparrizos, 2024) for Affiliation F1 ($F1_A$), Standard F1 ($F1$), and VUS-PR. For Temporal F1, we follow the implmentation of Sarfraz et al. (2024).

- **Standard-F1** The Standard F1-score is a widely used metric that provides a harmonic mean of precision and recall. It is calculated using point-wise True Positives (TP), False Positives (FP), and False Negatives (FN).
- **F1-T** Temporal F1, as described by Sarfraz et al. (2024), is a range-based metric that evaluates anomaly detection performance by considering the temporal context of anomalies. It is a vari-

ant of the F1-score that addresses common issues in time series evaluation, such as overlapping predictions and temporal proximity.

- **Affiliation-F ($F1_A$)** Affiliation F1 is a distance-based metric that measures the "affiliation" or proximity between the ground truth and predicted anomaly points. It is designed to be less sensitive to minor temporal shifts in the predicted anomalies. The score is calculated by finding the optimal one-to-one mapping between the ground truth and detected anomalies and then computing the F1-score based on these affiliations (Huet et al., 2022).
- **VUS-PR** (Volume Under Surface - Precision/Recall) is a threshold-independent, parameter-free metric for time series anomaly detection. Unlike point-wise metrics, VUS-PR is robust to time lags and measures the area under a 3D surface plot of precision, recall, and a buffer parameter (Paparrizos et al., 2022). It addresses the limitations of standard F1 scores by creating a continuous buffer region around each anomaly, thus providing a more reliable and nuanced evaluation of model performance.

D.4 Training Details

Pre-training Setup The pretraining setup for our time series model is built around a transformer architecture. This encoder features 8 transformer layers, each with 8 attention heads. The internal dimension (`d_model`) of the model is 512, which is then projected down to a dimension of 256 (`d_proj`). The input time series is divided into patches of size 16. The model is trained using the `AdamW` optimizer with a learning rate of 5e-4 and a weight decay of 1e-5. The total loss is a sum of two components: a Mean Squared Error loss for a masked reconstruction task and a Cross-Entropy loss for an anomaly detection task. Training runs for a maximum of 50 epochs with a batch size that starts at 64 but is adjusted dynamically, and it includes an early stopping mechanism that halts training if the validation loss doesn't improve for 7 epochs.

Pre-training Dataset Details We trained our model **only** on our custom synthetic dataset, which comprises a total of 2.5B data points. This dataset is composed of a vast number of individual time series with widely varying lengths. Figure 8 illustrates the distribution of these lengths. As the histogram shows, our pre-training curriculum follows a long-tailed distribution. It is dominated by a large volume of shorter series, which teaches the model common, localized patterns. Critically, it also includes a significant and diverse tail of longer series, with lengths extending up to 10,000 time steps. This diversity is fundamental to our approach. By pre-training on series of vastly different scales, the model learns to capture patterns across multiple temporal ranges and becomes well-equipped to handle the variable context lengths required for different downstream datasets.

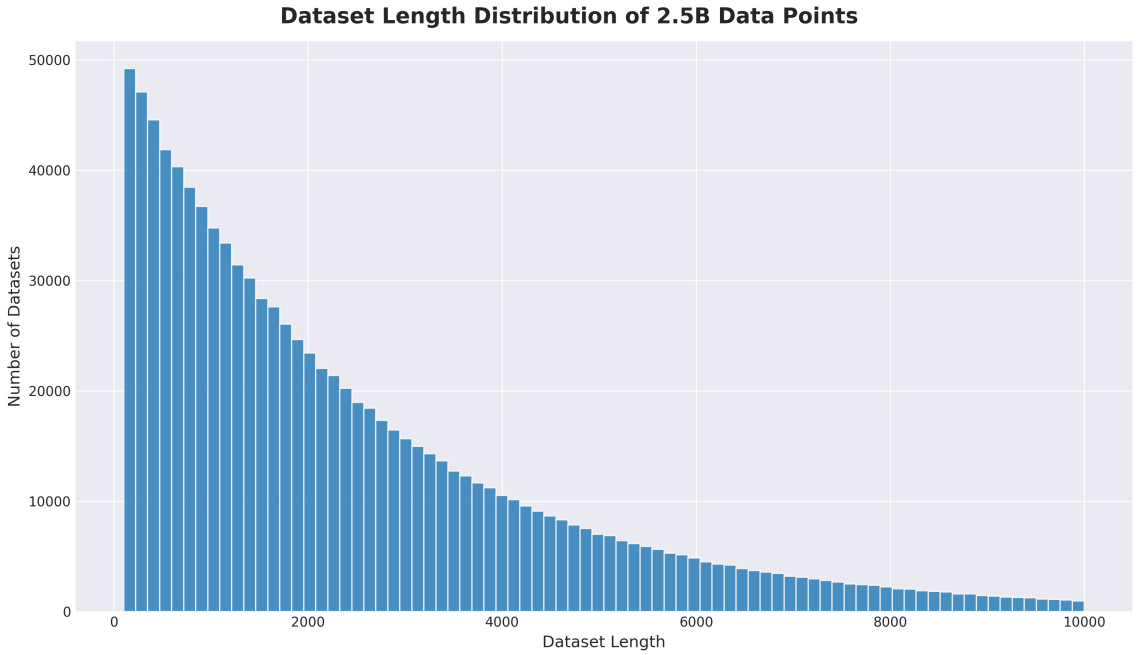

Figure 8: Distribution of time series lengths within our 2.5B point synthetic pre-training dataset. The histogram follows a long-tailed distribution, demonstrating that the pre-training curriculum is highly diverse. It contains a large volume of shorter series (under 4,000 steps) to teach common patterns, while also including a significant number of longer series (up to 10,000 steps) to ensure the model learns long-range temporal dependencies.

E EXTENDED RESULTS AND ANALYSIS

E.1 FULL RESULTS

This section provides the complete, unabridged performance results that support the summary claims made in the main text.

Experimental Setup and Zero-Shot Protocol Our evaluation involves two distinct comparisons: (1) a direct **zero-shot** comparison against other foundation models, and (2) a comparison against **full-shot** models where specialized baselines are trained on the target data. We emphasize that **our model remains strictly zero-shot in all settings**, rigorously testing its out-of-the-box performance. In a direct comparison against other leading foundation models, our model demonstrates clear state-of-the-art (SOTA) capabilities. On the univariate benchmarks, our model ranks first in an overwhelming **41** cases and second in **6**. Even more impressively, when benchmarked against full-shot models that have the advantage of training on target-specific data, our zero-shot model proves highly competitive, securing the top rank in **28** univariate evaluations and second place in another **5**.

Context Window Size Parameters for Main Results For the main results presented in Table 1, a context window size was selected for each dataset based on the analysis in Appendix E.3 to optimize performance. Specifically, for most univariate datasets, a window size of **5k** was used. Exceptions were made for the **NAB** dataset, where a smaller **1k** window was found to be optimal, and the long-series **Power** dataset, where the maximum tested **13k** window yielded the best results. For all five multivariate datasets, a context window of **13k** was applied to best capture their complex, inter-channel dependencies.

E.2 CONTEXTUAL ANALYSIS

To provide a controlled environment for testing our model's contextual understanding, we generated a new suite of specialized, unseen test datasets. The objective was to create two distinct sets: one containing only **point anomalies** and another containing only **contextual anomalies**. This section details their construction process.

General Construction Process Each dataset was generated using the framework described in the main paper, with a crucial modification: only one type of anomaly was injected per set. We first synthesized a complex "normal" baseline series, combining trend, seasonal, and noise components. We then injected specific anomalies into these clean series to create our test cases. These datasets were not used in any part of the pre-training process.

Point Anomaly Datasets Point anomalies are defined as short-term, localized deviations that can be identified by comparing a data point to its immediate neighbors, without requiring long-range context.

Contextual Anomaly Datasets Contextual anomalies are defined as deviations from a long-term, established pattern, such as a disruption in a seasonal cycle. Detecting them requires the model to understand the global structure of the time series.

Dataset Summary The final collection consists of two distinct sets of time series, with their key characteristics summarized in Table 9.

Table 9: Quantitative comparison on specialized Point and Contextual anomaly datasets. The table is grouped by anomaly type, with metrics listed vertically for each. Our model demonstrates competitive performance on point anomalies and substantially superior performance on contextual anomalies across all metrics. Best results in each row are highlighted in **bold**.

Type	Metric	Our Model	Chronos	DADA	MOMENT	TSPulse	Time MOE	TimesFM
Point	Affiliation-F	**0.912**	0.899	0.823	0.886	0.733	0.793	0.889
	$F1_T$	**0.604**	0.441	0.387	0.551	0.214	0.303	0.446
	Standard-F1	**0.521**	0.352	0.121	0.472	0.090	0.149	0.397
	VUS-PR	**0.666**	0.293	0.396	0.538	0.063	0.190	0.385
Contextual	Affiliation-F	**0.949**	0.804	0.721	0.813	0.730	0.756	0.792
	$F1_T$	**0.781**	0.174	0.227	0.284	0.210	0.269	0.154
	Standard-F1	**0.827**	0.154	0.048	0.172	0.088	0.078	0.140
	VUS-PR	**0.879**	0.108	0.132	0.169	0.056	0.063	0.101

E.3 Window Size Sensitivity Analysis

In this section, we show the detailed performance of our model across different context window sizes (from 1k to 13k) for each of the four primary evaluation metrics. The following figures provide a per-dataset breakdown, which supports the summarized analysis presented in the main paper.

The results in Figures 9 through 12 empirically validate our key finding: the optimal context length is task-dependent, and datasets with long-term or complex structures see a clear benefit from larger window sizes.

- **Positive Scaling Trend:** A strong positive correlation between window size and performance is evident for several datasets across most metrics. For example, **Power**, **UCR**, **MGAB**, **SMD**, and **SMAP** all demonstrate a general upward trend, especially on the F1-T, Standard-F, and VUS-PR metrics. This confirms that for these series, a larger context provides a more robust understanding of "normalcy", leading to better anomaly detection.
- **Flat Performance on Short Series:** In contrast, datasets with inherently short time series, such as **YAHOO**, **NEK**, and **TODS**, show a flat performance profile. Their scores remain largely unchanged regardless of the window size. This is the expected behavior, as the length of the time series itself acts as the natural context limit, and the model correctly avoids computing attention over non-existent data.
- **Task-Dependent Fluctuation:** Other datasets, like **NAB**, **PSM**, and **SWaT**, exhibit more fluctuating or non-monotonic behavior. For these, the ideal window size varies, with performance sometimes peaking at intermediate lengths. This underscores the value of having a flexible architecture where the context window can be tuned as a hyperparameter to achieve optimal results for a specific task.
- **Metric Sensitivity:** It is also noteworthy that the 'Affiliation-F' metric (Figure 9) generally appears less sensitive to changes in window size compared to the other three metrics. This suggests that while a larger context may be crucial for the precise, point-wise accuracy captured by metrics like 'Standard-F1', the broader, proximity-based evaluation of 'Affiliation-F' is less affected.

These detailed results collectively reinforce the conclusion that the model's ability to handle extensive, variable-length contexts is a powerful and necessary feature for a general-purpose time-series anomaly detector.

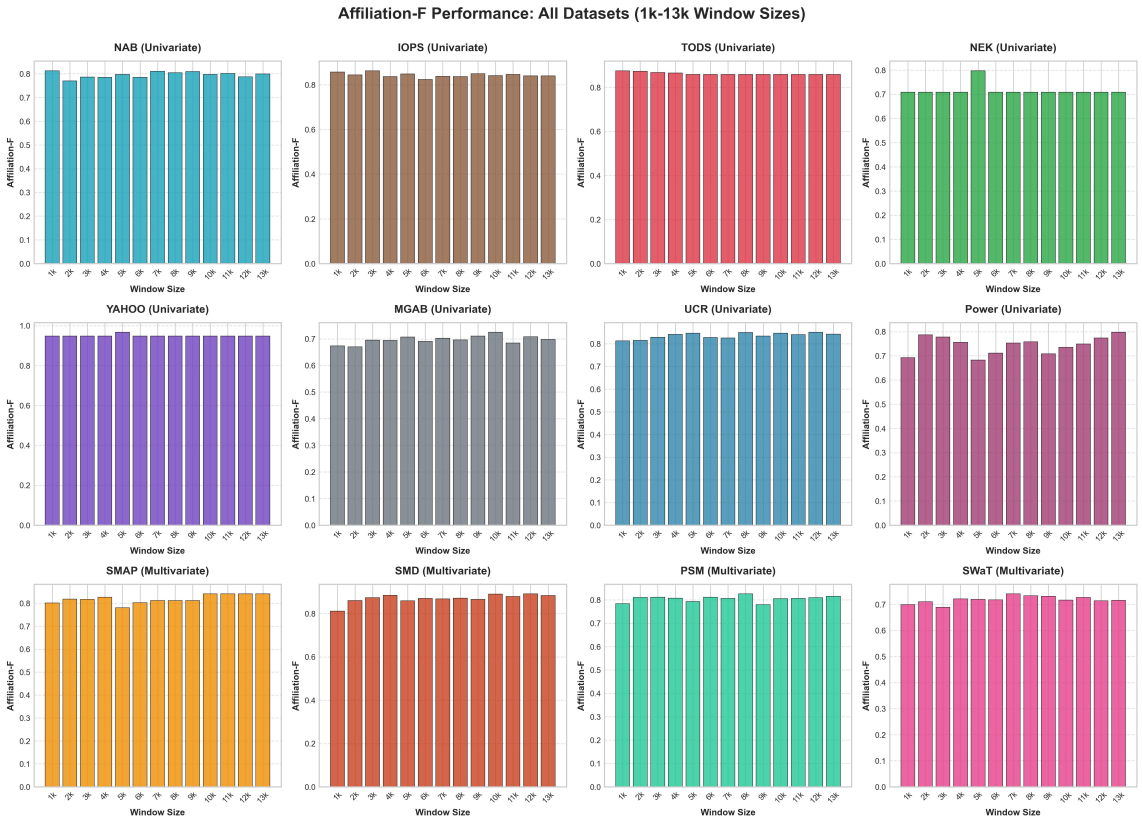

Figure 9: Affiliation-F performance across all 14 datasets as a function of the input window size from 1k to 13k.

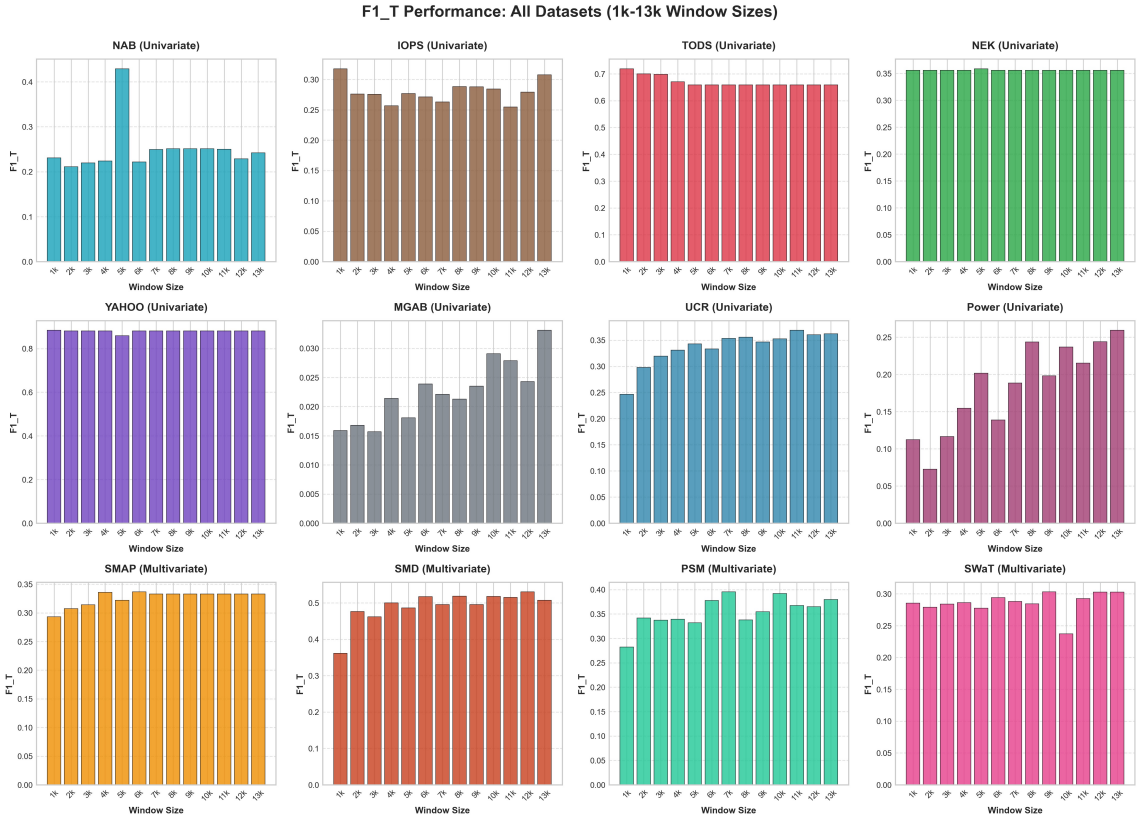

Figure 10: $F1_T$ performance across all 14 datasets as a function of the input window size from 1k to 13k.

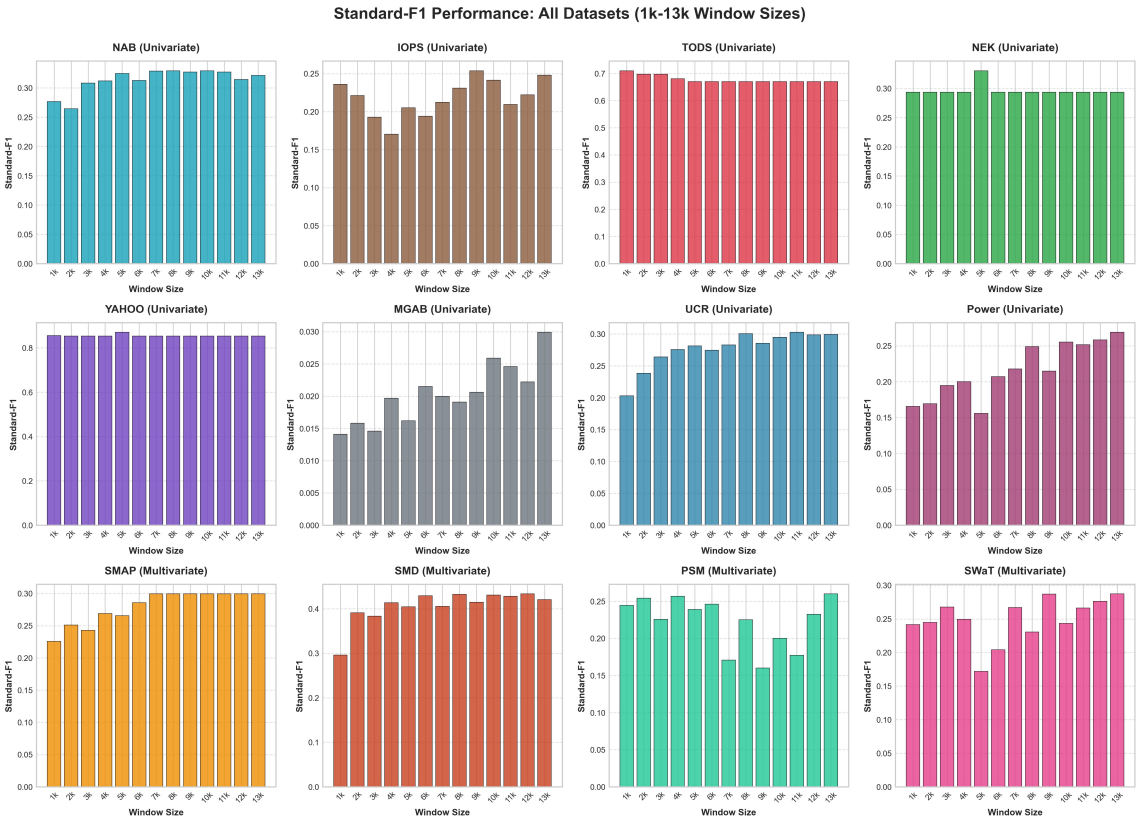

Figure 11: Standard-F1 performance across all 14 datasets as a function of the input window size from 1k to 13k.

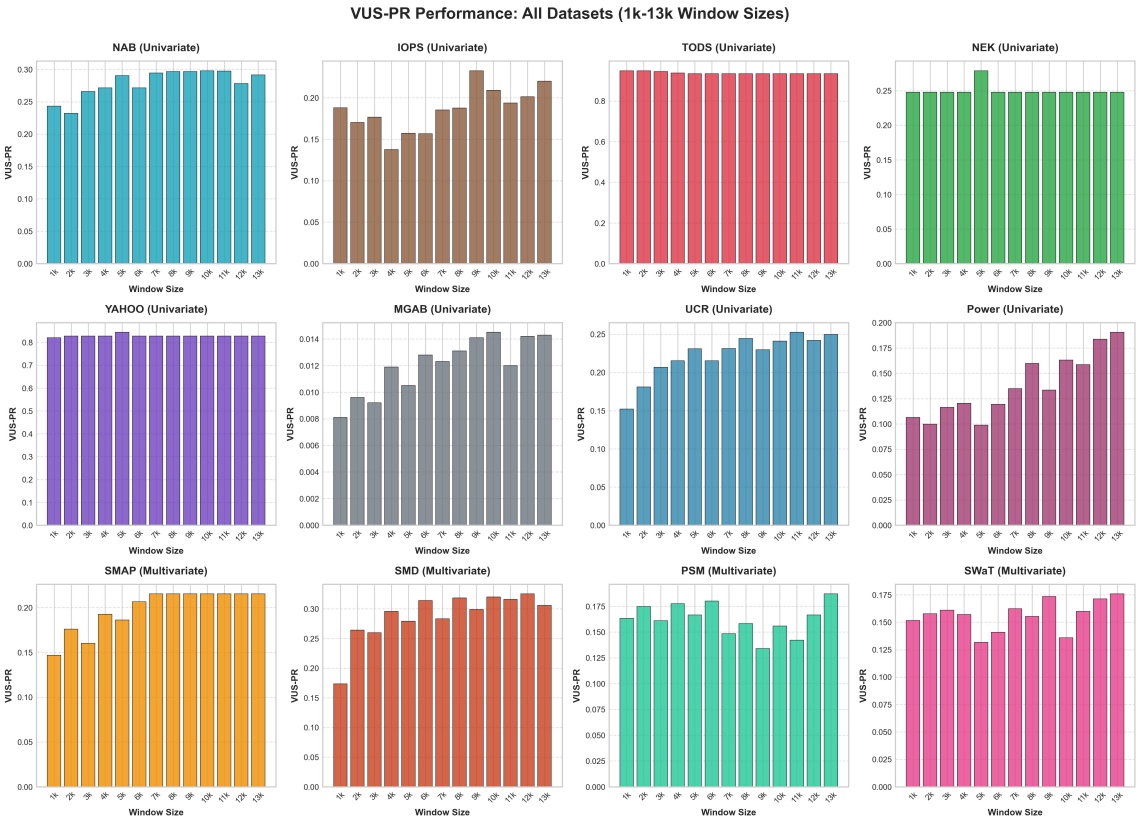

Figure 12: VUS-PR performance across all 14 datasets as a function of the input window size from 1k to 13k.

Table 10: Impact of Context Window Size: A comprehensive performance comparison of our model with varying context window sizes across all univariate and multivariate benchmark datasets. Best results for each dataset-metric combination are highlighted in **red**, and second-best are in blue.

Metric	Model	Univariate Datasets									Multivariate Datasets					Total	Total
		IOPS	MGAB	NAB	NEK	Power	SED	TODS	UCR	YAHOO	MSL	PSM	SMAP	SMD	SWaT	1st	2nd
Affiliation-F	1k	85.64	67.32	**81.28**	70.87	69.30	87.07	**87.56**	81.34	94.73	78.50	78.36	80.16	81.11	69.93	02	02
	2k	84.41	66.97	77.01	70.87	78.73	91.51	87.24	81.54	94.79	79.63	81.04	81.80	85.99	71.00	00	04
	3k	**86.25**	69.50	78.60	70.87	77.83	92.15	86.73	82.88	94.79	80.27	81.12	81.77	87.30	68.87	01	02
	4k	83.61	69.41	78.48	70.87	75.57	94.57	86.48	84.12	94.79	80.75	80.75	82.68	88.48	72.12	00	04
	5k	84.79	70.69	79.70	**79.73**	68.30	96.87	85.91	84.63	**96.65**	79.90	79.35	78.04	85.94	71.93	02	00
	6k	82.30	69.08	78.49	70.87	71.10	96.92	85.91	82.75	94.79	79.90	81.11	80.25	87.07	71.79	00	02
	7k	83.72	70.24	81.00	70.87	75.32	96.92	85.91	82.55	94.79	79.90	80.67	81.23	86.76	**74.03**	01	03
	8k	83.65	69.58	80.40	70.87	75.77	95.22	85.91	84.95	94.79	79.90	**82.56**	81.23	87.14	73.29	01	04
	9k	84.90	71.07	80.97	70.87	70.83	97.66	85.91	83.46	94.79	79.90	77.94	81.23	86.59	73.10	00	04
	10k	84.02	**72.45**	79.74	70.87	73.48	**97.77**	85.91	84.70	94.79	**81.13**	80.55	**84.10**	89.03	71.65	04	03
	11k	84.54	68.39	80.08	70.87	74.96	97.36	85.91	84.03	94.79	**81.13**	80.62	**84.10**	87.85	72.69	02	02
	12k	83.91	70.79	78.67	70.87	77.39	95.27	85.91	**85.06**	94.79	**81.13**	80.94	**84.10**	**89.09**	71.41	04	02
	13k	83.98	69.82	79.96	70.87	**79.73**	95.44	85.91	84.24	94.79	**81.13**	81.61	**84.10**	88.29	71.55	03	03
F1_T	1k	**31.77**	01.59	23.07	35.60	11.22	51.63	**71.91**	24.66	**88.38**	39.60	28.22	29.30	36.13	28.53	03	01
	2k	27.60	01.68	21.11	35.60	07.27	57.90	69.97	29.79	88.12	40.45	34.16	30.72	47.63	27.91	00	03
	3k	27.58	01.57	21.94	35.60	11.66	58.75	69.80	31.96	88.12	39.99	33.75	31.43	46.19	28.39	00	02
	4k	25.68	02.14	22.36	35.60	15.44	64.61	67.01	33.10	88.12	**42.47**	33.95	33.59	49.98	28.60	01	03
	5k	27.70	01.81	**42.90**	**35.87**	20.17	69.43	65.89	34.30	85.86	41.54	33.19	32.22	48.64	27.75	02	01
	6k	27.13	02.39	22.17	35.60	13.87	72.40	65.85	33.31	88.12	41.54	37.75	**33.66**	51.73	29.42	01	03
	7k	26.31	02.21	24.95	35.60	18.83	70.80	65.85	35.33	88.12	41.54	**39.53**	33.28	49.54	28.80	01	03
	8k	28.84	02.13	25.09	35.60	24.36	70.86	65.85	35.57	88.12	41.54	33.77	33.28	51.83	28.44	00	04
	9k	28.78	02.35	25.12	35.60	19.80	**74.65**	65.85	34.68	88.12	41.54	35.46	33.28	49.54	**30.30**	02	04
	10k	28.42	02.91	25.08	35.60	23.66	73.61	65.85	35.27	88.12	41.54	39.22	33.28	51.77	23.73	00	06
	11k	25.45	02.79	24.99	35.60	21.51	71.50	65.85	**36.89**	88.12	41.54	36.75	33.28	51.52	29.27	01	03
	12k	27.90	02.43	22.86	35.60	24.40	69.70	65.85	36.03	88.12	41.54	36.48	33.28	**53.02**	30.28	01	05
	13k	30.77	**03.31**	24.19	35.60	**25.92**	70.33	65.85	36.23	88.12	41.54	37.98	33.28	50.73	30.28	02	06
Standard-F1	1k	23.61	01.41	27.68	29.38	16.57	51.89	**71.00**	20.30	85.54	27.22	24.47	22.56	29.59	24.17	01	02
	2k	22.10	01.58	26.45	29.38	16.92	58.24	69.76	23.84	85.33	28.58	25.43	25.11	39.08	24.48	00	02
	3k	19.26	01.46	30.84	29.38	19.46	59.15	69.74	26.39	85.33	29.48	22.58	24.27	38.33	26.76	00	01
	4k	17.04	01.97	31.20	29.38	20.02	65.02	68.05	27.58	85.33	**30.66**	25.68	26.89	41.35	24.96	01	02
	5k	20.51	01.62	32.46	**33.05**	15.59	69.88	67.01	28.13	**87.02**	29.95	23.91	26.54	40.45	17.18	02	01
	6k	19.40	02.15	31.27	29.38	20.70	72.71	67.01	27.46	85.33	29.95	24.61	28.57	42.90	20.40	00	03
	7k	21.23	02.00	32.90	29.38	21.76	71.16	67.01	28.28	85.33	29.95	17.09	**29.93**	40.56	26.70	01	02
	8k	23.08	01.91	32.91	29.38	24.88	71.26	67.01	30.04	85.33	29.95	22.50	**29.93**	43.25	23.07	01	05
	9k	**25.38**	02.06	32.70	29.38	21.47	**75.00**	67.01	28.53	85.33	29.95	16.00	**29.93**	41.44	28.69	03	03
	10k	24.14	02.59	**32.94**	29.38	25.52	74.07	67.01	29.50	85.33	29.95	20.01	**29.93**	43.08	24.36	02	04
	11k	20.96	02.46	32.72	29.38	25.15	71.89	67.01	**30.26**	85.33	29.95	17.74	**29.93**	42.80	26.63	02	02
	12k	22.21	02.22	31.45	29.38	25.84	70.16	67.01	29.85	85.33	29.95	23.27	**29.93**	**43.33**	27.63	02	03
	13k	24.81	**02.99**	32.13	29.38	**26.88**	70.76	67.01	29.92	85.33	29.95	**26.00**	**29.93**	42.05	**28.73**	05	03
VUS-PR	1k	18.80	0.8100	24.32	24.78	10.64	48.68	**94.89**	15.22	82.02	17.45	16.33	14.68	17.35	15.16	01	01
	2k	17.03	0.9600	23.23	24.78	09.97	59.79	94.86	18.11	82.78	18.23	17.48	17.59	26.41	15.77	00	03
	3k	17.66	0.9200	26.58	24.78	11.64	65.57	94.46	20.69	82.78	18.94	16.10	16.02	25.97	16.09	00	02
	4k	13.74	01.19	27.13	24.78	12.05	73.53	93.80	21.53	82.78	**20.45**	17.76	19.27	29.57	15.70	01	02
	5k	15.71	01.05	29.02	**27.88**	09.88	80.75	93.46	23.09	**84.41**	19.61	16.67	18.62	27.89	13.17	02	01
	6k	15.67	01.28	27.13	24.78	11.96	86.59	93.46	21.52	82.78	19.61	18.01	20.66	31.37	14.08	00	05
	7k	18.53	01.23	29.43	24.78	13.50	84.32	93.46	23.14	82.78	19.61	14.85	**21.53**	28.31	16.24	01	03
	8k	18.75	01.31	29.66	24.78	15.98	86.40	93.46	24.45	82.78	19.61	15.82	**21.53**	31.83	15.53	01	03
	9k	**23.26**	01.41	29.67	24.78	13.35	**92.86**	93.46	22.99	82.78	19.61	13.39	**21.53**	29.91	17.35	03	04
	10k	20.91	**01.45**	**29.79**	24.78	16.30	91.36	93.46	24.10	82.78	19.61	15.59	**21.53**	32.00	13.59	03	05
	11k	19.38	01.20	29.74	24.78	15.86	87.48	93.46	**25.26**	82.78	19.61	14.22	**21.53**	31.59	16.00	02	04
	12k	20.13	01.42	27.82	24.78	18.38	85.60	93.46	24.20	82.78	19.61	16.65	**21.53**	**32.51**	17.13	02	04
	13k	22.00	01.43	29.14	24.78	**19.05**	86.77	93.46	24.99	82.78	19.61	**18.70**	**21.53**	30.58	**17.58**	04	06

E.4 Analysis for Ablation Study on Pre-training Data

In this section, we provide a detailed, per-dataset analysis of the ablation study on our pre-training data, which supports the weighted average results discussed in the main paper.

Experimental Setup To rigorously validate our data generation framework, we conducted a controlled experiment. We trained our model on three distinct pre-training datasets, each standardized to 350M data points. A completely identical training protocol—including the same model architecture, hyperparameters, and number of training epochs—was used for each run to isolate the impact of the data itself. The three datasets were:

1. **Our Synthetic Data:** Generated entirely by our proposed framework, including our custom, context-aware anomaly injection techniques.
2. **Our Synthetic Data + DADA Injection:** The same base time series as above, but with anomalies introduced using the generic DADA injection method described by Shentu et al. (2024).
3. **Real-world Data + DADA Injection:** A dataset created by applying DADA injection to real-world time series from the Monash forecasting repository Godahewa et al..

Univariate Setting Justification This experiment was conducted exclusively in a univariate setting for two primary reasons. First, the large-scale real-world dataset available for creating a comparable baseline (*Monash*) is predominantly comprised of univariate series. Second, the DADA anomaly injection technique, as described in their original paper, is designed for and implemented on univariate time series. This constraint ensures a fair and direct comparison between the different data generation strategies.

Detailed Results and Analysis Table 11 presents the full, per-dataset results for the nine univariate benchmarks used in this study. These results offer a more granular view than the weighted averages in the main text.

The per-dataset results first confirm the main conclusion: the model pre-trained on augmented real-world data demonstrates significantly inferior performance across most datasets and metrics, particularly on the F1-based scores. This validates our hypothesis that a purpose-built synthetic curriculum is superior to simply augmenting existing real-world series.

More interestingly, the table reveals the nuances behind the weighted average comparison between our two synthetic strategies. While the "Our Synthetic Data + DADA Injection" strategy secures more first-place finishes on a per-dataset basis (e.g., strong performance on IOPS and NAB), our custom injection method ("Our Synthetic Data") achieves higher scores on other key datasets like TODS and YAHOO. The fact that our method yields a better weighted average on $F1_T$ and Standard-F1 (as mentioned in the main paper) suggests that its performance is more stable or that it excels on datasets that have a greater influence on the overall average. This highlights a critical trade-off: DADA's generic injections can be highly effective for specific data profiles, whereas our context-aware injection methods appear to provide a more consistent and robust performance across a wider range of scenarios, leading to better overall performance on the most stringent metrics. Ultimately, this detailed analysis reinforces that our end-to-end synthetic data generation framework provides the most effective training curriculum for achieving state-of-the-art zero-shot performance.

Table 11: Performance comparison across different models and metrics. Best results for each dataset-metric combination are highlighted in **red**, and second-best are in blue.

Metric	Model	Datasets									Total 1st	Total 2nd
		IOPS	MGAB	NAB	NEK	Power	SED	TODS	UCR	YAHOO		
Affiliation-F	Our Synthetic Data	89.37	68.55	88.74	79.27	63.31	89.24	**83.26**	**83.88**	92.35	02	05
	Our Synthetic Data + DADA Injection	**90.50**	**68.67**	**88.80**	79.60	**78.52**	**94.04**	80.92	82.43	**93.63**	06	03
	Real-world Data + DADA Injection	70.98	67.59	81.99	**82.61**	70.73	62.18	55.56	74.80	68.41	01	01
F1_T	Our Synthetic Data	36.08	01.08	25.69	55.06	06.23	53.92	**58.76**	31.59	**85.99**	02	04
	Our Synthetic Data + DADA Injection	**53.11**	**01.91**	**34.91**	59.59	**13.16**	**61.45**	57.66	**32.74**	68.57	06	03
	Real-world Data + DADA Injection	06.80	01.35	23.18	**70.65**	10.01	0.1700	09.67	05.25	05.37	01	02
Standard-F1	Our Synthetic Data	30.63	01.13	30.12	50.89	17.39	54.18	**61.66**	24.38	**82.16**	02	06
	Our Synthetic Data + DADA Injection	**46.46**	**01.74**	**34.65**	48.90	**19.53**	**61.43**	59.62	**26.20**	65.66	06	02
	Real-world Data + DADA Injection	11.02	01.32	26.17	**66.97**	17.09	03.08	11.99	03.83	03.53	01	01
VUS-PR	Our Synthetic Data	24.07	0.7000	27.16	48.66	09.66	61.63	88.62	**20.59**	74.68	01	07
	Our Synthetic Data + DADA Injection	**45.24**	**0.9500**	**32.22**	48.52	**12.60**	**65.09**	**93.48**	19.17	**75.67**	07	01
	Real-world Data + DADA Injection	08.88	0.6400	24.54	**69.75**	11.09	06.69	45.82	02.12	12.18	01	01

E.5 Additional Analysis for Scaling Laws

In this section, we provide the full, per-dataset results for our investigation into the impact of pre-training data scale on model performance. These granular results support the weighted average trends and conclusions presented in the main paper.

Experimental Setup To investigate the effect of pre-training data scale, we trained our model on increasingly larger subsets of our synthetic dataset: 350M, 700M, and the full 2.5B data points. Each model was trained using an identical protocol to isolate the effect of the data volume. Due to the predominantly univariate nature of the large-scale datasets used to construct our synthetic curriculum, this scaling analysis was conducted exclusively on the nine univariate benchmark datasets.

Detailed Results and Analysis The results, presented in Table 12, confirm the existence of a strong and positive scaling law. As the volume of pre-training data increases, the model's overall performance consistently improves. This is most evident in the "Total 1st" place rankings, where the full **2.5B** model overwhelmingly outperforms the smaller models across all four metrics, securing the top rank in 24 out of 36 total evaluations. While the general trend is clear, the per-dataset results reveal some interesting nuances. The scaling is not perfectly monotonic for every dataset-metric combination. For instance, the **700M** model achieves the best 'F1-T score on the IOPS and YAHOO datasets, and the **350M** model shows strong performance on the NEK dataset. These variations likely stem from a combination of dataset-specific characteristics and the inherent stochasticity of the training process. However, the dominant performance of the 2.5B model in the aggregate rankings strongly validates our approach of leveraging a large-scale pre-training curriculum. It also suggests that the model's capabilities are not yet saturated, with the potential for further improvement with even more data.

Table 12: Performance comparison across different models and metrics. Best results for each dataset-metric combination are highlighted in **red**, and second-best are in blue.

Metric	Model	Datasets									Total 1st	Total 2nd
		IOPS	MGAB	NAB	NEK	Power	SED	TODS	UCR	YAHOO		
Affiliation-F	**2.5B**	84.79	**70.69**	79.70	**79.73**	68.30	**96.87**	**85.91**	**84.63**	**96.65**	06	01
	700M	86.46	68.87	**86.43**	72.74	**73.02**	92.07	83.95	82.23	93.74	02	05
	350M	**88.24**	68.19	86.21	79.27	63.30	89.21	83.22	82.49	92.35	01	03
F1_T	**2.5B**	27.70	**01.81**	**42.90**	35.87	**20.17**	**69.43**	**65.89**	**34.30**	85.86	06	00
	700M	**40.56**	01.49	27.82	42.31	05.13	59.02	64.07	28.88	**86.88**	02	05
	350M	36.08	01.08	25.69	**55.06**	06.23	53.92	58.76	31.59	85.99	01	04
Standard-F1	**2.5B**	20.51	**01.62**	**32.46**	33.05	15.59	**69.88**	**67.01**	**28.13**	**87.02**	06	01
	350M	**30.63**	01.13	30.12	**50.89**	**17.39**	54.18	61.66	24.38	82.16	03	01
	700M	30.08	01.51	32.17	42.68	12.63	59.31	66.45	22.71	83.92	00	07
VUS-PR	**2.5B**	15.71	**01.05**	29.02	27.88	**09.88**	**80.75**	**93.46**	**23.09**	**84.41**	06	01
	700M	**26.51**	0.7200	**30.18**	36.27	08.51	67.37	91.62	18.35	78.48	02	05
	350M	24.07	0.7000	27.16	**48.66**	09.66	61.63	88.62	20.59	74.68	01	03

E.5.1 Additional Analysis for Ablation Study

Ablation Study of Anomaly/Reconstrution Head To analyze the contribution of our model's key components, we conducted an ablation study on the representative UCR dataset. We compare three distinct versions: (1) the **Full Model**, which includes both our dedicated anomaly head and the auxiliary reconstruction head; (2) **Anomaly Head Only**, where the reconstruction task is removed; and (3) **Reconstruction Only**, where scores are derived from reconstruction error. The results, presented in Table 13, reveal the critical synergy between our model's two heads. The Full Model substantially outperforms both ablated versions

across all metrics. Interestingly, the Anomaly Head Only model sees a near-total collapse in performance, performing significantly worse than even the Reconstruction Only model. This result strongly suggests that the auxiliary reconstruction task is not merely helpful, but essential. It provides a foundational learning signal that teaches the model to understand the basic structure of the time series, without which the dedicated anomaly head cannot function effectively. Therefore, our architecture's state-of-the-art performance stems directly from the combination of these two components: the reconstruction head learns the representation, and the anomaly head refines it to achieve superior detection capabilities.

Table 13: Ablation study results on the UCR dataset. The synergy of the Full Model provides the best performance, while the reconstruction head proves essential for the anomaly head to function effectively.

Model Version	**Affiliation-F**	**F1$_T$**	**Standard-F1**	**VUS-PR**
Full Model	**0.846**	**0.343**	**0.281**	**0.231**
Anomaly Head Only	0.709	0.043	0.024	0.014
Reconstruction Only	0.742	0.109	0.075	0.044